# An approach for long-term, multi-probe Neuropixels recordings in unrestrained rats

Thomas Zhihao Luo[1†*], Adrian G. Bondy[1†*], Diksha Gupta[1], Verity A. Elliott[1], Charles D. Kopec[1], Carlos D. Brody[1,2]

[†]These authors contributed equally; [1]Princeton Neuroscience Institute, Princeton, NJ 08544; [2]Howard Hughes Medical Institute, Princeton University, Princeton 08544, USA; *For correspondence: zhihaol@princeton.edu (TZL); abondy@princeton.edu (AGB)

## Abstract

The use of Neuropixels probes for chronic neural recordings is not yet widespread and initial studies leave questions about long-term stability and probe reusability unaddressed. Here we demonstrate a new approach for chronic Neuropixels recordings over a period of months in freely moving rats. Our approach allows multiple probes per rat and multiple cycles of probe reuse. We found that hundreds of units could be recorded for multiple months, but that yields depended systematically on anatomical position. Explanted probes displayed a small increase in noise compared to unimplanted probes, but this was insufficient to impair future single-unit recordings. We conclude that cost-effective, multi-region, and multi-probe Neuropixels recordings can be carried out with high yields over multiple months in rats or other similarly sized animals. Our methods and observations may facilitate the standardization of chronic recording from Neuropixels probes in freely moving animals.

## Introduction

Behavior depends on the concurrent spiking activity of many neurons across large distances in the brain. Therefore, tools that improve our ability to sample neuronal activity at the temporal resolution of action potentials and also with large spatial coverage will expand our ability to answer key neuroscience questions. The recent development of a silicon microelectrode array, the Neuropixels probe (Jun et al., 2017; Mora Lopez et al., 2017), is a significant step forward in that direction. Its high channel count allows sampling from hundreds of neurons per probe, on-probe amplification and digitization allows for low-noise data transmission, and a small footprint allows multiple probes to simultaneously survey regions across the brain. Given these advantages, the use of Neuropixels probes in acute experiments in head-fixed mice has become widespread and standardized (Allen et al., 2019; Steinmetz et al., 2019; The International Brain Laboratory et al., 2020).

Chronic implantations are particularly crucial for experiments that examine behaviors involving unrestrained movement, such as some perceptual decision-making (Brunton et al., 2013) tasks, exploration (Tervo et al., 2014), navigation (Ito et al., 2015), escape (Juavinett et al., 2019), foraging (Davidson & El Hady, 2019), and prey-capture (Hoy et al., 2019). However, the deployment of these probes in experiments requiring chronic implantation has remained very limited (Juavinett et al., 2019; Jun et al., 2017; Krupic et al., 2018). A previous study tracked the stability of neural signals acquired from the rat medial prefrontal cortex (Jun et al., 2017). This study found that across implants, there was no significant degradation of signals across two months. A different study reported that 20-145 single units could be isolated in the mouse visual cortex, hippocampus, and midbrain from one to two weeks after surgery (Juavinett et al., 2019). This latter study used an implantation strategy that allowed the probe to be recovered and reused, which can save laboratories

substantial resources given the significant cost and limited production of the probes. Moreover, this study reported that high-quality neural signals could be observed after re-implantation of two explanted probes.

Several outstanding issues need to be addressed before the enormous potential for chronic implantation of Neuropixels probes can be fully realized. First, the long-term yield across different brain regions is unknown because prior chronic studies recorded from a small set of brain regions using test-phase probes (Juavinett et al., 2019; Jun et al., 2017). The stability of spiking signals is likely to vary across regions because the brain is not mechanically uniform, with different viscoelastic properties and levels of respiration- and cardiac-related movement in different regions (Bayly et al., 2005; Budday et al., 2015; MacManus et al., 2018; Sloots et al., 2020). Second, the feasibility of probe reuse remains uncertain. The reusability of explanted probes was assessed previously by comparing the frequency and signal-to-noise of spiking events recorded from two re-implanted probes (Juavinett et al., 2019). However, neural signals can be highly variable, and can be different across separate implantations for reasons unrelated to the probes themselves. To assess the feasibility of probe re-use, it is necessary to also measure the performance of the explanted probe independent of neural signals. Moreover, techniques that allow probe recovery have not been validated for multi-month recordings, or validated in rats, which can be ten times larger in size than mice and can generate much larger impact forces that can damage probe signals.

To address these issues, we developed and validated an approach for recoverable chronic implants that is robust to forces generated by rats over multiple months and compact enough for multiple probes to be implanted on the same rat. We designed a probe holder, inspired by (Juavinett et al., 2019), that can be produced using a 3D printer and allows the probe to be easily retrieved for reuse. Using this approach, we recorded from eighteen rats, each implanted with up to three probes simultaneously, while they performed a cognitively demanding task for multiple hours daily without human supervision and at a level similar to their pre-implantation baseline. Recordings were made broadly throughout the rat forebrain and midbrain. From these, we reached three conclusions: first, over a hundred single units can be recorded per probe over multiple months. Second, the stability of long-term recording depends systematically on the dorsoventral and anteroposterior position in the brain, with greater stability for more anterior and ventral regions. This finding could guide future experiments and probe development. Finally, to test the feasibility of re-using Neuropixels probes after extended periods of implantation, we directly measured the input-referred noise of explanted probes in saline after prolonged implantation. We found only modest increases in noise across multiple (up to three) cycles of implantation and explantation, demonstrating the practicality of probe re-use. Taken together, these results further demonstrate the enormous potential of Neuropixels probes for experiments requiring unrestrained movement, and validate new methods for deploying these probes to full advantage in chronic preparations.

# Results

### Holder design

We developed a design (Figure 1) for mounting and enclosing a Neuropixels 1.0 probe, with the goals to minimize the size and weight of the implant, allow the probe to be easily recovered at the end of the experiment, and be robust to impact forces that rats can generate (Methods).The probe was permanently glued to a custom-designed adapter (Figure 1A), which was attached to an internal holder through a dovetail joint and screws (Figure 1B-C). The holder was then attached by screws to an external chassis (Figure 1D-E). During surgery, the holder was used to stereotaxically manipulate the probe, and the external chassis was cemented to the animal's skull. At the end of an experiment, the screws between the internal holder and external chassis were removed allowing the probe to be explanted (Figure 1H). By unscrewing the adapter from the holder, a nearly bare probe can then be recovered. All parts were produced in-house using 3D stereolithography printers. The maximum dimensions of the assembly were 43 mm (height), 25 mm (width), and 10.5 mm (depth), with a weight of 2.6 g. The size and weight of the design provides sufficient protection to

the probe from the impact force that a rat can generate while allowing for a rat to comfortably carry additional probes or hardware for neural perturbation.

Eighteen rats were implanted with one or more Neuropixels probes. One rat was implanted with three probes simultaneously, and two rats with two concurrent probes (Figure 1F-H), all enclosed in explantable probe holders. The probes targeted a large number of cortical and subcortical brain regions, including prefrontal, visual, somatosensory, and retrosplenial cortex, as well as the basal ganglia, amygdala, and the superior and inferior colliculi. See Methods for complete list of recording sites and Figure 2--supplement 1 for example histological images. See also Figure 4--supplement 1 for list of each individual implantation and its outcome.

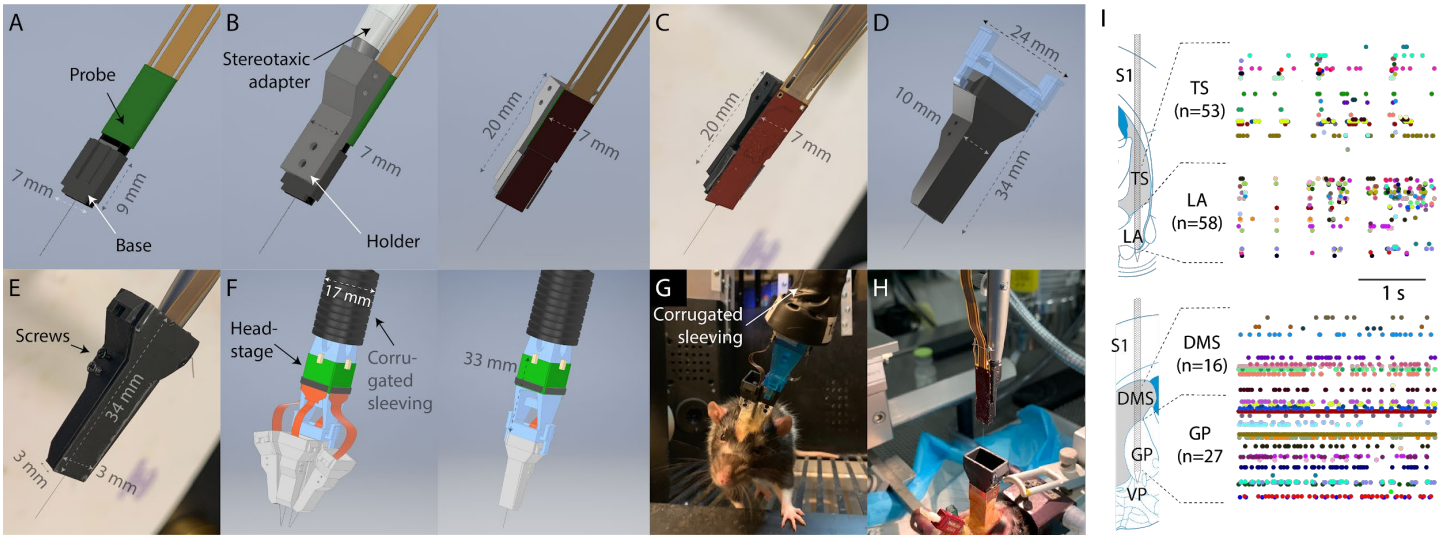


**Figure 1. A compact system for chronic recording and subsequent probe recovery.** To prevent bonding of the probe to the skull, the probe was fully enclosed in a chassis. During surgery, the chassis was bonded to the skull so the probe can later be detached and recovered. The assembly was sufficiently compact for multiple probes to be implanted in the same animal. A) To prepare a probe for implantation, it was first mounted to a 3D-printed base that served as a dovetail adapter. B) Schematic of the base mating with a 3D-printed holder through a dovetail joint, and the holder was attached to a commercially available stereotaxic holder. The schematic is shown from two different views. C) A photograph of a mounted probe. D) The entire apparatus was then enclosed with a 3D-printed external chassis. During the surgery, the chassis, but not the holder, was fixed to the skull surface using adhesive cement and acrylic, and therefore the holder could be separated from the chassis. E) A photograph of an enclosed probe, with screws securing the chassis to the internal holder visible. F) A 3D-printed headstage-mount can have up to four headstages mounted to it and mates directly with external chassis through snap-on holders. The headstage-mount was fixed to a corrugated plastic sleeving, which protects the cable from small bending radii. G) A rat with two probes implanted. H) A photograph of the explantation of a probe. Also visible is an interconnect for an optical fiber (red). I) Simultaneous recordings from two Neuropixels probes in a moving rat. Top: recording from tail of striatum (TS) and lateral amygdala (LA, 2.2 mm anterior to Bregma, 5.0 mm lateral). Bottom: recording from dorsomedial striatum (DMS) and globus pallidus (GP; 0.6 mm posterior to Bregma, 4.0 mm lateral). Images and schematic are adapted from (Paxinos & Watson, 2006). Colored dots indicate spike times.

## Stability of spiking signals

To quantify the stability of spiking signals across days, we periodically performed short recordings of approximately ten minutes from the group of 384 recording sites either closest or second closest to the tip of the probe shank (“bank 0” and “bank 1”, respectively). A total of 46,929 isolated units were recorded across 141 recording sessions, 18 animals, and 15 unique stereotaxic coordinates. All but one probe implanted were Neuropixels 1.0 probes, and all results were identical if the testing-phase (“3A”) probe was excluded. Spike sorting was performed using Kilosort2 (Pachitariu, 2020). To facilitate comparison across datasets and eliminate subjectivity in spike sorting (Harris et al., 2000; Wood et al., 2004), we used default parameters and no manual curation. Isolated units that exhibited sufficiently few refractory period violations were classified as “single units” (SUs) and the rest as “multi-units” (MUs) (Methods).

Even among implants targeting the same brain area, there was variability in the time course of unit counts between animals, as seen in other reports of chronic Neuropixels recording (Juavinett et al., 2019; Jun

et al., 2017). For example, among three implants targeting medial frontal cortex (Figure 2A), the number of SUs recorded on the day of the surgery varied by a factor of two (~100 versus >200). In one of those implants, the number of SUs initially decreased and then increased. Variability can also be observed among implants targeting motor cortex and striatum (Figure 2B) and in implants targeting the ventral striatum (Figure 2C).

Averaged across implants, the total number of isolated units (including SUs and MUs) began at 578 ± 52 (mean ± 1 s.e.m.) on the day after implantation, decreased over the subsequent days, and stabilized after approximately one week, to roughly one half the number of units that could be initially recorded (8 to 120 days after implant: 278 ± 22; Figure 2D-E). After this initial loss during the first week, the number of total units, as well as the number of SUs, remained stable for up to four months, the longest time span for which we have sufficient data (ANOVA, single-factor (days), for only data > 7 days: tested on the number of units *p=0.895* and on the number of SUs: *p=0.581*). The fraction of units that were SUs did not change over time (ANOVA, *p=0.331*). The activity levels of the isolated units and the size of the spike waveforms also remained stable (Figure 2--supplement 2; ANOVA, event rate: *p=0.188*; peak-to-peak amplitude: *p=0.290*). The expected yield of over 200 isolated units (100 SUs) per bank per probe over the period of a week to four months after implantation indicates this approach likely provides sufficient signal for studying coordinated, population-level activity during behavior.

The loss of units over time can be described quantitatively using a sum of two exponential decay terms (Methods), which can be interpreted as two subpopulations with different time constants of disappearance. Model estimates (Figure 2--supplement 3) indicate that half of the population (units: 0.50 [0.42, 0.59]; SUs: [0.39, 0.54]) was associated with a fast exponential change rate (units: -0.49 [$-10^{6}$, -0.15]; SUs: -1.48 [$-10^{6}$, -0.27]). A change rate of ~-0.5 indicates that within a week of the implant, this subpopulation declined to less than 5% of its initial value, thereby accounting for the rapid decrease in yield within the first week. The subpopulation with faster decay might be neurons that were acutely damaged during probe insertion (Bjornsson et al., 2006). The remaining subpopulation had a change rate that was nearly zero: -0.0001 [-0.0025, $-10^{-6}$]; SUs: -0.0005 [-0.0025, $-0.10^{-6}$]), accounting for the stable yield after the first week.

We further sought to identify the experimental factors that might affect the time course of unit loss. Signal stability depended on anatomical position, notably on the dorsoventral (DV) position in the brain (Figure 2G-I). The number of units recorded from the electrodes in the most superficial two millimeters of brain tissue (corresponding to the dorsal cerebral cortex in all our recordings) declined steadily over several months until a near-complete disappearance of units. The ratio of the average number of units >30 days after implantation to the average number of units on the first day after implantation was 0.18 (bootstrapped 95% CI = [0.10, 0.29]; SUs only: 0.17 [0.07, 0.30]). In contrast, the electrodes more than two millimeters below the brain surface, which targeted the striatum and ventral medial frontal cortex in the majority of implants, were associated with a significantly more modest degradation that eventually stabilized. The ratio of the average number of units >30 days after implantation to the average number of units on the first day was 0.50 [0.38, 0.63] (SUs only: 0.54 [0.40, 0.71]). Fitting the sum-of-exponentials model to this data, there was a significant difference in the decay rate of the more slowly decay subpopulation (*p=0.002,* bootstrap test; SUs: *p=0.001*; Figure 2G-I; and Figure 2--supplement 3). This led to a significant difference in the model's effective time constant, which is the number of days until 1/e, or 37%, of the units remained, between the superficial and deeper electrodes (Figure 2I). These results indicate that long-term stability depends on dorsoventral location.

The stability of neural signals also depended on the probe's position along the animal's anteroposterior (AP) axis: a difference could be observed between our recordings anterior and posterior to Bregma (Figure 2J-L). Recordings from more posterior sites were associated with fewer initial clusters (*p=0.010*, rank-sum test), which could be in part due to a lower neuron density in the posterior structures compared to the anterior structures that we recorded from (Erö et al., 2018). There was also a more severe degradation in yield in the posterior areas, with a virtually complete loss of units after one month. The ratio of the total number of units 30 days or more after implantation to the unit count 1 day after implantation was 0.09 (95% CI = [0.04, 0.22]) for posterior recordings and 0.50 [0.40, 0.63] for the anterior recordings. The same ratio for the number of SUs only was 0.06 [0.00, 0.21] for posterior recordings and 0.53 [0.38, 0.72] for anterior recordings. Fitting the sum-

of-exponentials model to this data, there was a significant difference in the decay rate of the more slowly decay subpopulation (*p=0.002,* bootstrap test; SUs: *p=0.001*) and also in the initial unit count(*p=0.005*; SUs: *p=0.003*; Figure 2J-L; and Figure 2--supplement 3). The effective time constant of the sum-of-exponentials model was significantly different between units recorded from anterior and posterior electrodes (Figure 2L). These results indicate that long-term stability depends on anteroposterior location.

The relative number of units corresponding to the fast- and slowly-decaying subpopulations did not significantly vary across brain regions along either anatomical axis, nor did the rate of decay of the fast population (Figure 2--supplement 3). This suggests that the rapid decline in yield observed in the days after surgery may be due to a process that is relatively uniform across brain regions.

In addition to DV and AP positions, there are likely other factors that also affect the time course of unit loss, such as the ML position. In addition to anatomical position, the position of a recording site on the probe shank might be relevant because the probe is more flexible near its tip. Greater flexibility allows the shank to move more easily with the surrounding brain tissue and therefore may lead to less tissue damage over time (Lecomte et al., 2018). The shank orientation (i.e, the angle of the probe's plane relative to the brain) might also be relevant because the probe's width is three times its thickness (70 µm vs. 24 µm), making it ~27 times more flexible in the axis perpendicular to its plane. If the relative motion between the probe and the brain is anisotropic, the orientation of the probe's more flexible axis could affect yield stability. .

To infer the relationship between these experimental factors and the unit count over time, the sum-of-exponentials model was next fitted using all these factors as regressors. To take advantage of the larger sample size and the greater variation in the experimental factors across individual electrodes, the model was fitted to the unit count of each electrode in each recording session (Methods). The elaborated model assumes two subpopulations of units ($\alpha$ and $1\text{-}\alpha$) whose decay rates are each a linear combination of the regressors, including a constant term unique to each population ($\beta_{fast}$ for the $\alpha$ population and $\beta_{slow}$ for the $1\text{-}\alpha$ population). In this way, the decay rates of the two subpopulations could vary across electrodes while exhibiting a constant difference ($\beta_{fast} - \beta_{slow}$). The regressors included AP (mm anterior), DV (mm relative to brain surface), ML (mm from midline), SP (shank position, mm above tip) and SO (shank orientation, whether the shank was parallel to the brain's coronal, as opposed to, sagittal plane). The initial unit count ($N_1$) was also a linear combination of the regressors, excluding SP and SO because their contribution to the initial yield is not readily interpretable. The three parameters ($\alpha$, $\beta_{fast}$, and $\beta_{slow}$) were fixed across electrodes to limit the number the number of parameters and because previous observations indicated that the decay rate of only the more stable subpopulation depended on the experimental factors (Figure 2--supplement 3).

Because the regressors are partly correlated, estimation depends on what other regressors are included in the model. To make the inference more reliable, all-subset variable selection was performed to exhaustively identify the subset of regressors that best predicted the data. We also included model variants in which we substituted the continuous regressor $DV$ with $DV>\text{-}2mm$, which approximately separates dorsal cerebral cortex from deeper areas of the brain in our recordings, to examine whether unit count is better predicted by whether an electrode is in dorsal cortex rather than by its depth.

Among 448 variable subsets (Methods), the five model variants with the lowest out-of-sample log-likelihood (LL) included the $AP$ and $ML$ variables as predictors for the initial unit count ($N_1$) (Figure 2N), such that a larger initial unit count was associated with a more anterior and a more medial position. The best model also included the regressors $AP$, $DV>\text{-}2$, and $SO$ (shank orientation) for the change rate term ($k$) (Figure 2O), such that a slower loss of units was associated with an electrode that was more anterior, below dorsal cortex, and on a shank whose plane is parallel to the brain's sagittal plane. The coefficients in the change rate term were similar in the order of magnitude to the that of baseline change rate of the more slowly decaying subpopulation ($\beta_0^{slow}$), indicating that the experimental factors tested here affected the slow disappearance of units over multiple weeks and months rather than the rapid disappearance during the first few days after implantation. If any coefficient had a magnitude that is intermediate between $\beta_0^{fast}$, and $\beta_0^{slow}$, then it would suggest that the experimental factors affected the fast and slowly decaying subpopulations differently, rather than in the same way, as it is assumed by the model. Finally, the model variant without any of the experimental factors as regressors (i.e., with only the

constant terms) was ranked 396 out of 448, indicating that the factors are relevant for predicting unit loss over time.

The best model included five (non-constant) regressors. Examining each group of model variants with four, three, two, and one regressors revealed that the regressors in the best *n*-regressor model is a superset of the regressors in the best (*n-1*)-regressor model. This nesting of regressors is not required by the all-subset variable selection process (such as when the regressors are shuffled), and it provides a list of regressors ordered by decreasing importance for predicting unit count: $N_1$-$AP$, $k$-$DV$>-2, $N_1$-$ML$, $k$-$AP$, $k$-$SO$. Taken together, the results indicate that a higher initial unit count is associated with electrodes that are more anterior and medial, and that a slower decay rate is associated with electrodes that are below dorsal cortex, further anterior, and on a shank parallel to the sagittal plane.

Finally, the loss of spiking signals that we observe at first appears to contrast with a previous study reporting chronic recording in rat medial prefrontal cortex (mPFC) (Jun et al., 2017), where no such loss was found. However, when we examine just the mPFC recordings in our dataset (prelimbic cortex and medial orbital cortex, n=4 rats), no degradation in the number of total units was apparent over a two month span, and the number of SUs and event rate actually increased (Figure 2--supplement 4). This finding further demonstrates the dependence of signal stability on anatomical AP and DV positions, because our recordings from mPFC were the most anterior (AP = 4.0 mm from Bregma) and were taken 1.8 mm or more below the brain surface.

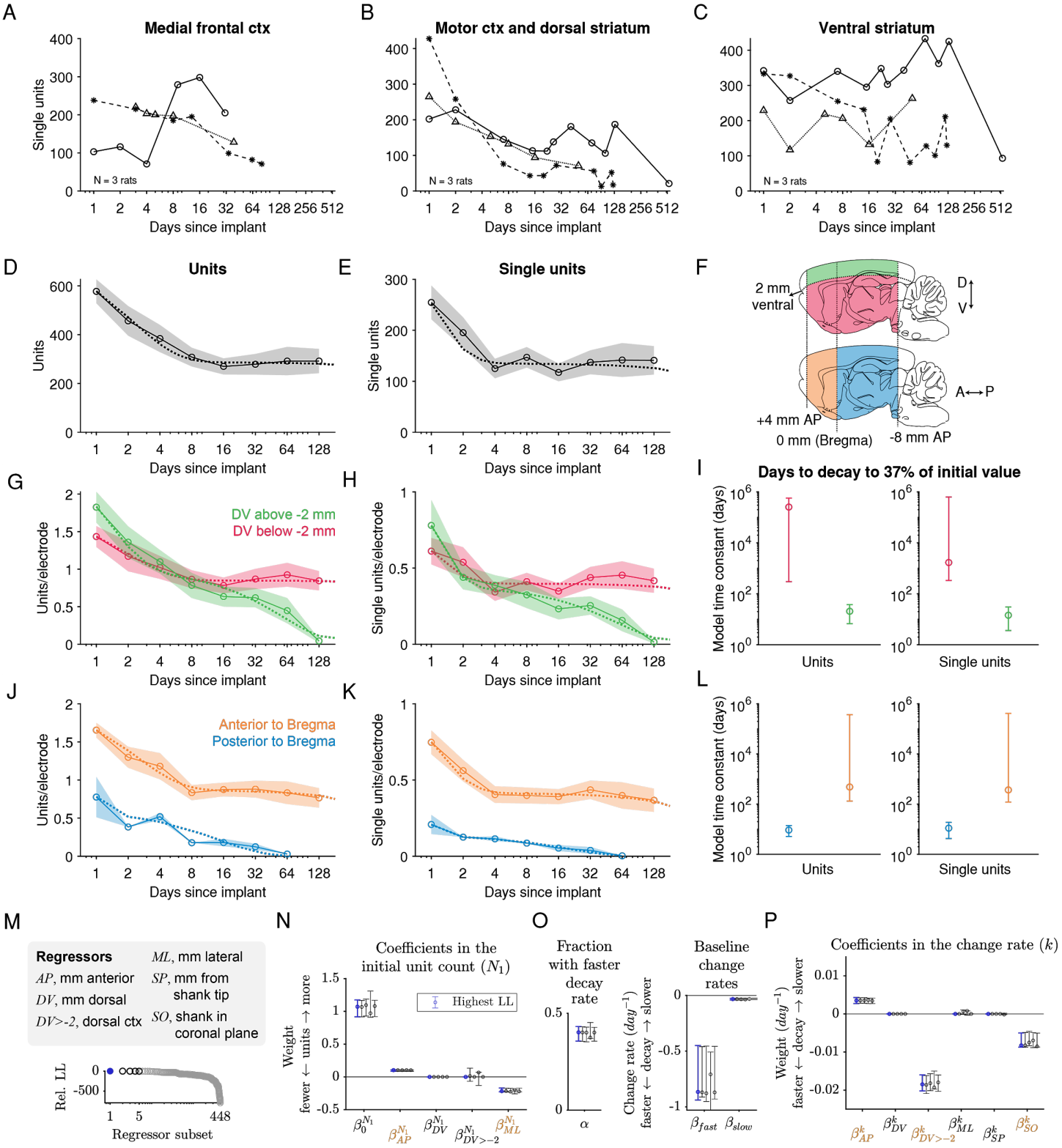


**Figure 2. After an initial loss of units, spiking signals can be maintained >60 days in anterior, deeper brain regions.** A) Recordings from the medial frontal cortex (including secondary motor, cingulate,, and medial orbital cortices) across three example animals. Each combination of marker and line types indicates one animal. B) Recordings from secondary motor cortex and anterior dorsal striatum. C) Recordings from anterior ventral striatum. D) The number of units recorded. Shading represents mean +/- 1 s.e.m. across recording sessions. The dashed line is the fit of a sum of two exponential decay terms, representing two subpopulations with different time constants of decay. E) The number of single units. F) To explore the dependence of signal stability on anatomical position, units were separated into two groups along either the dorsoventral (DV) axis or the anteroposterior (AP) axis. G) The number of units recorded either more superficial to or deeper than 2 mm below the brain surface, normalized by the number of electrodes in the same region. H) Similar to G, but showing the number of single units. I) The model time constant is the inferred number of days after implantation when the count of units (or single units) declined to *1/e*, or ~0.37, of the count on the first day after implant. The 95% confidence intervals were computed by drawing 1000 bootstrap samples from the data. J-L) Similar to G-I, but for data grouped according to their position along the anterior-

posterior axis of the brain. (M) A sum-of-exponentials regression model was fit to the number of units recorded from each electrode in each session (N = 57,586 recordings) to infer the relationship between experimental factors and unit loss over time. Continuous regressors $AP$, $DV$, $ML$, and $SP$ indicate an electrode's position in millimeters anterior, dorsal, lateral, and from the shank tip, respectively. Categorical regressors $DV{>}{-2}$ and $SO$ indicate whether an electrode is in the dorsal cortex or on a probe whose shank is in the coronal plane, respectively. Model variants with different subsets of regressors were ordered by relative out-of-sample log-likelihood (LL). The five subsets with the highest LL are shown in subsequent panels. (N) Coefficients in the equation term indicating the initial unit count ($N_1$) from the five regressors subsets with the highest LL. Initial unit count consistently depends on *AP* and *ML* (orange), which are included and significantly nonzero in the top five models. Error bars indicate 95% bootstrap confidence intervals. For continuous regressors, the dimension of the coefficient is $mm^{-1}$. (O) About 40% ($\alpha$) of the units disappeared rapidly with a baseline change rate of -0.87 ($k_{fast}$), and the remaining disappeared more slowly with a baseline change rate of -0.03 ($k_{slow}$). (P) Decay rates depended consistently on the regressors $AP$, $DV{>}{-2}$ (whether the unit was in dorsal cortex), and $SO$ (whether the shank was parallel to the coronal plane), which are included and have a significantly nonzero coefficient in the top five models. For continuous regressors, the dimension of the coefficient is $mm^{-1}$. (D-E) N = [12, 8, 20, 18, 32, 20, 13, 16] recording sessions for each bin. (G-H) DV [-10, -2] mm: N = [12, 8, 19, 18, 32, 20, 13, 16]; DV [-2, 0] mm: N = [6, 4, 11, 7, 14, 10, 8, 5]. (J-K) AP [-8, 0] mm: N = [2, 1, 5, 1, 8, 4, 1]; AP [0, 4] mm: N = [10, 7, 15, 17, 24, 16, 12, 16].

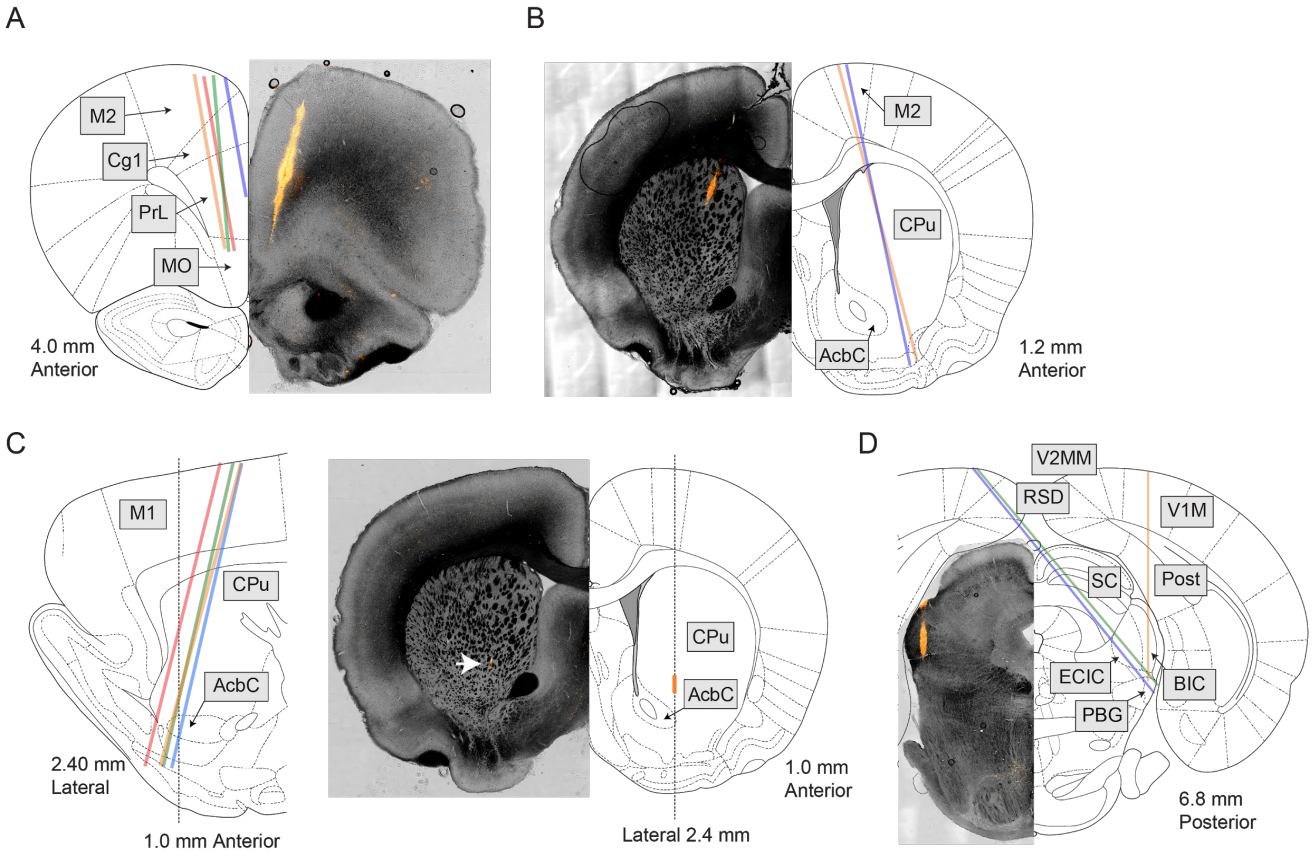


**Figure 2--supplement 1. Example histological images of probe tracks.** A) Four probes were implanted in the medial frontal cortex. The coordinates targeted (but not necessarily realized) were 4.0 mm anterior from Bregma, 1.0 mm lateral, and 4.2 mm deep, -10° in the coronal plane. B) Two probes were implanted in anterior striatum and M2. The target coordinates were 1.9 mm anterior, 1.3 mm lateral, and 8.2 mm deep, and 15° in the coronal plane. C) Four probes were implanted in M1 and anterior striatum. The target coordinates were 0.0 mm anterior, 2.4 mm lateral, 8.2 mm deep, and 15° in the sagittal plane. While the probe was tilted in the sagittal plane, histological slices were taken in the coronal plane. D) Three probes were implanted in the midbrain with three different target coordinates: 1) 7.0 mm posterior, 3.0 mm lateral, and 5.8 mm deep. 2) 6.6 mm posterior, 1.6 mm lateral, and 7.8 mm deep, and -40° in the coronal plane. 3) 6.8 mm posterior, 1.7 mm lateral, and 8.0 mm deep, and -40° in the coronal plane. (A-D) Brain atlas was adapted from (Paxinos & Watson, 2006). AcbC, accumbens nucleus, core. BIC, nucleus of the brachium of the inferior colliculus. Cg1, cingulate cortex, area 1. CPu, caudate putamen. ECIC, external cortex of the inferior colliculus. MO, medial orbital cortex. M1, primary motor cortex. M2, secondary motor cortex. PBG, parabigeminal nucleus. Post, postsubiculum. PrL, prelimbic cortex. RSD, retrosplenial dysgranular cortex. SC, superior colliculus. V1M, primary visual cortex, monocular. V2MM, secondary visual cortex, mediomedial. A positive angle in the coronal plane indicates that the probe tip was more lateral than the insertion site at the brain surface, and a positive angle in the sagittal plane indicates that the probe tip was more anterior than the insertion site.

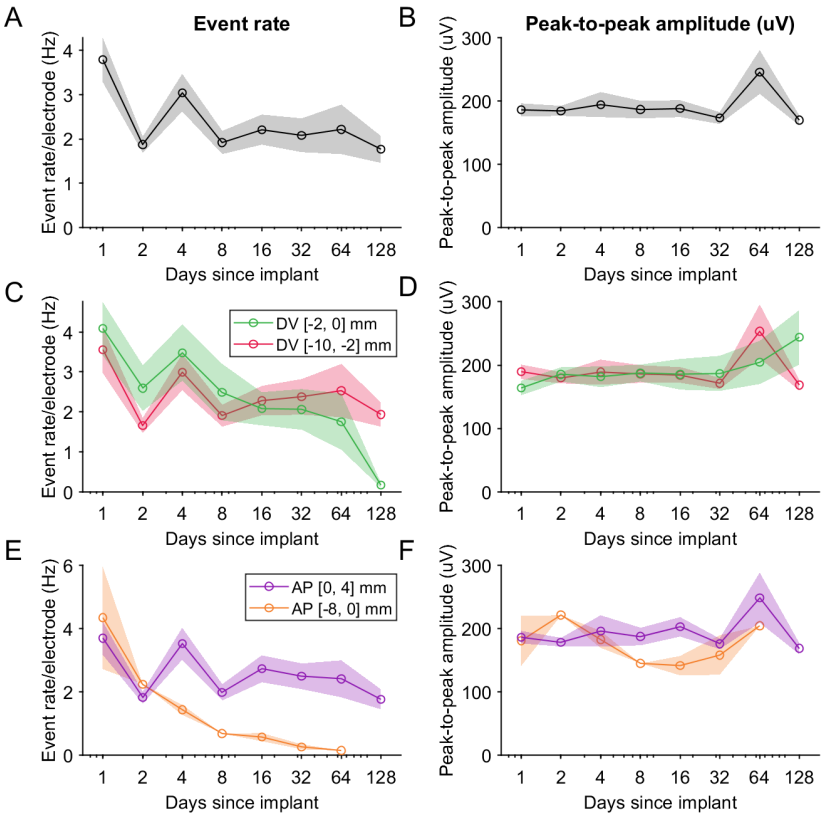


**Figure 2--supplement 2. The event rate and peak-to-peak amplitudes.** (A) The event rate (rate of all spikes across units). Shading represents mean +/- 1 s.e.m. across recording sessions. The transient increase in event rate in the time bin including days 3-5 is in part due to non-identical subsets of animals being included in different time bins, resulting in event rate variability due to differences in implanted brain region or arousal levels across animals. (B) The average peak-to-peak amplitude of the waveforms across units. (C-D) Event rate and peak-to-peak amplitude of units recorded either more superficial to or deeper than 2 mm below the brain surface, normalized by the number of electrodes in the same region. (E-F) Similar as (C-D), but for data grouped according to their position along the anterior-posterior axis of the brain.

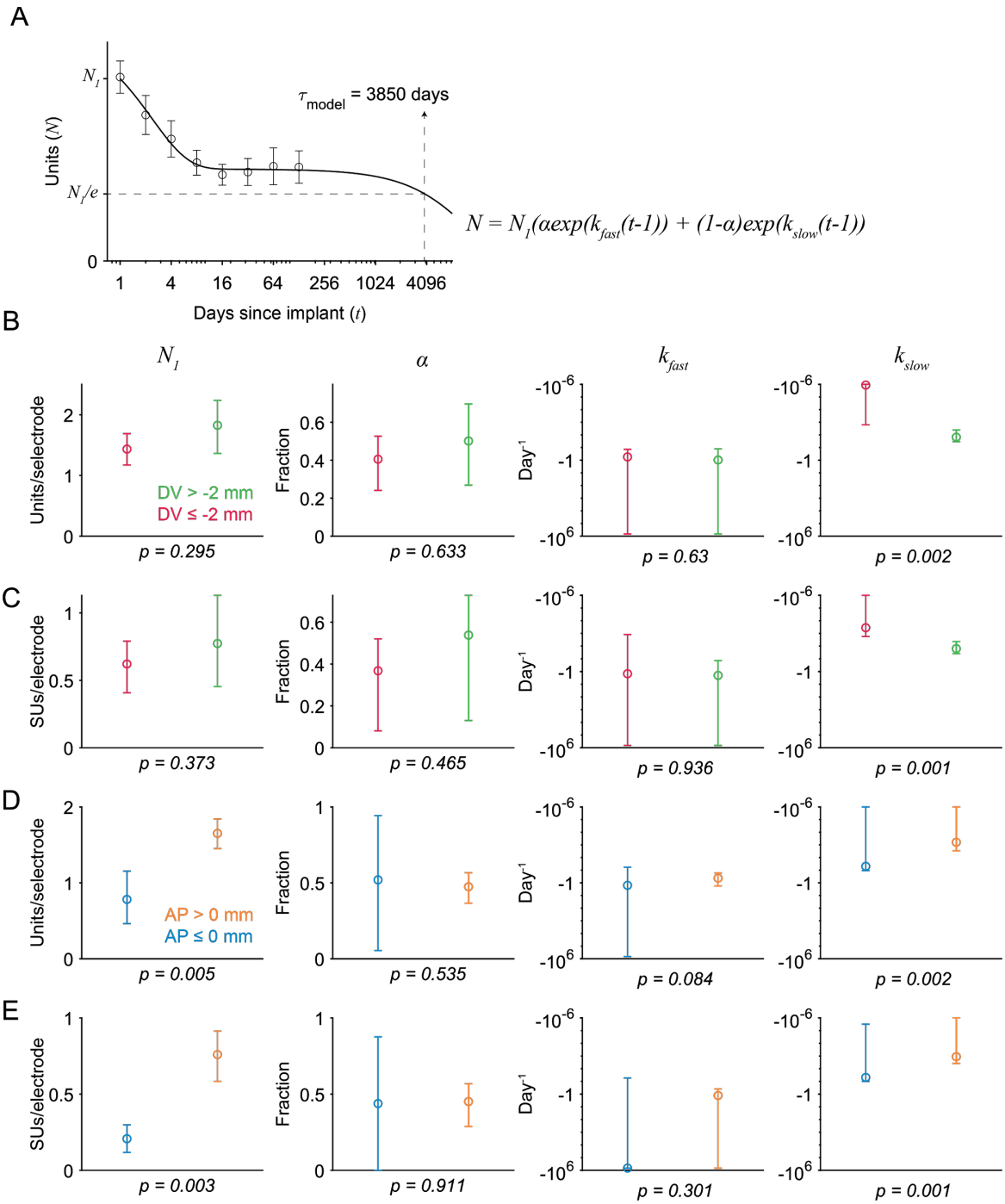


**Figure 2--supplement 3. Coefficient estimates of the sum-of-exponentials model used to describe unit loss over time.** The model postulates that the number of units (*N*) across days after implant (*t*) depended on exponential decay from the unit count on the first day after surgery ($N_1$). The term $\alpha$ is the fraction of the population whose exponential decay is parametrized by the time constant $\tau_{fast}$, and the remaining fraction (*1-α)* decays with a slower (i.e., larger) time constant $\tau_{slow}$. (A) The model time constant ($\tau_{model}$) is the inferred time when the unit count is *1/e* of the initial value. Markers and error bar indicate mean +/- 1 s.e.m. Solid line indicates the model fit. (B) Fits to the number of units recorded either more superficial to (green) or deeper than (red) 2 mm below the brain surface. The p-value was computed from a two-tailed bootstrap test. For each parameter, the p-value indicates the probability of the observed difference in the estimate between the model fit to the superficial units and the model fit to the deeper units, under the null hypothesis that the distributions of unit counts from superficial and deeper electrodes are identical. (C) Same as B, but for the number of single units. (D) Fits to the number of units recorded either more anterior to (orange) or posterior to (blue) Bregma. (E) Same as D, but for single units.

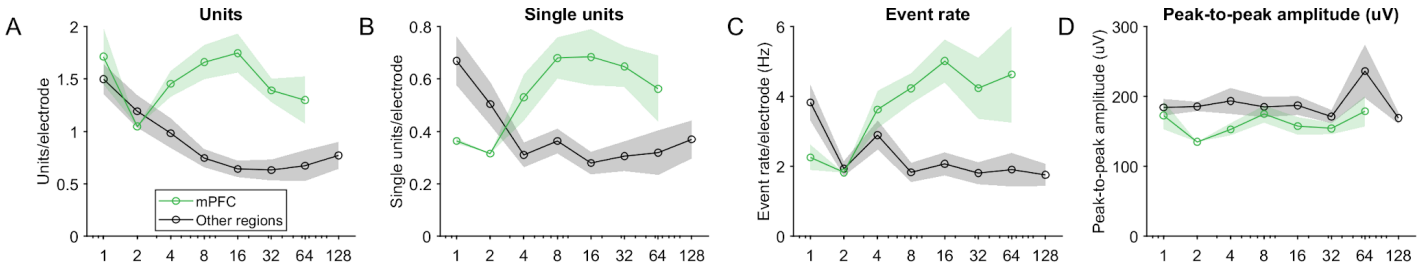


**Figure 2--figure supplement 4**. **No degradation of spiking signals was detected over two months in rat medial prefrontal cortex (mPFC), the brain region in which the stability of spiking signals was examined in** (Jun et al., 2017). mPFC was recorded from four probes (one probe/animal, N = (2, 1, 6, 3, 4, 6, 4) sessions, implanted 4.0 mm anterior to Bregma, 1.0 mm lateral, 10° in the coronal plane at the probe tip relative to DV axis) and from the electrodes of those probes located in prelimbic cortex or medial orbital cortex, as according to probe tracks in histological slices and referenced to (Paxinos & Watson, 2006). This finding contrasts with the clear signal degradation at all other recording sites. N = (12, 8, 20, 18, 32, 20, 13, 16). (A) The number of single units normalized by the number of electrodes in that brain region. (B) The number of single units. (C) The event rate. (D) The average peak-to-peak amplitude of waveforms.

## Behavioral performance while tethered for recording

Our motivation to chronically implant Neuropixels probes was to study coordinated neural activity during perceptual decision-making. Therefore, we sought to determine in what ways the recording procedure might change the animals' behavioral performance. In our approach, the cable connecting the headstage and the IMEC base station was encased in a split corrugated sleeving to limit the number of turns an animal could make in a single direction to three to five and thereby avoid small bending radiuses in the cable during hours of unsupervised recording (Figure 1F-G). We sought to quantify the effects of the tether's movement restriction on performance.

During the perceptual decision-making task, rats maintained their nose in a center port while two streams of auditory clicks played from loudspeakers on their left and right (Brunton et al., 2013). When the auditory stimulus ended, rats were rewarded for reporting which stream had played the greater number of clicks by placing their nose in a left or right port (Figure 3A). We found little or no significant degradation in a number of critical metrics of behavioral performance between when the rats were untethered and when they were tethered for recording. The median number of trials for which the rats were able to successfully maintain fixation in a given session remained similar (Figure 3B), indicating that the additional weight and constraint of the implant and tether did not affect the number of completed trials. The average percent correct was actually slightly higher during tethered performance (Figure 3C). The performance of individual rats was further quantified using a logistic function fit to their choice and the sensory evidence in each trial (Figure 3D; Methods). The slope of the logistic function (at the midpoint), which quantifies sensitivity to the sensory evidence, and the bias parameter were not significantly different (Figure 3E-F). Interestingly, tethered performance was associated with a lower lapse rate (Figure 3G). The lower median lapse rate and higher percentage correct could potentially be because after the surgery, the rats performed the task more frequently while tethered than untethered and therefore are more engaged while tethered and showed higher performance. These results indicate that the tethering process did not substantially impair the rats' motivation or their ability to successfully complete a cognitively demanding task.

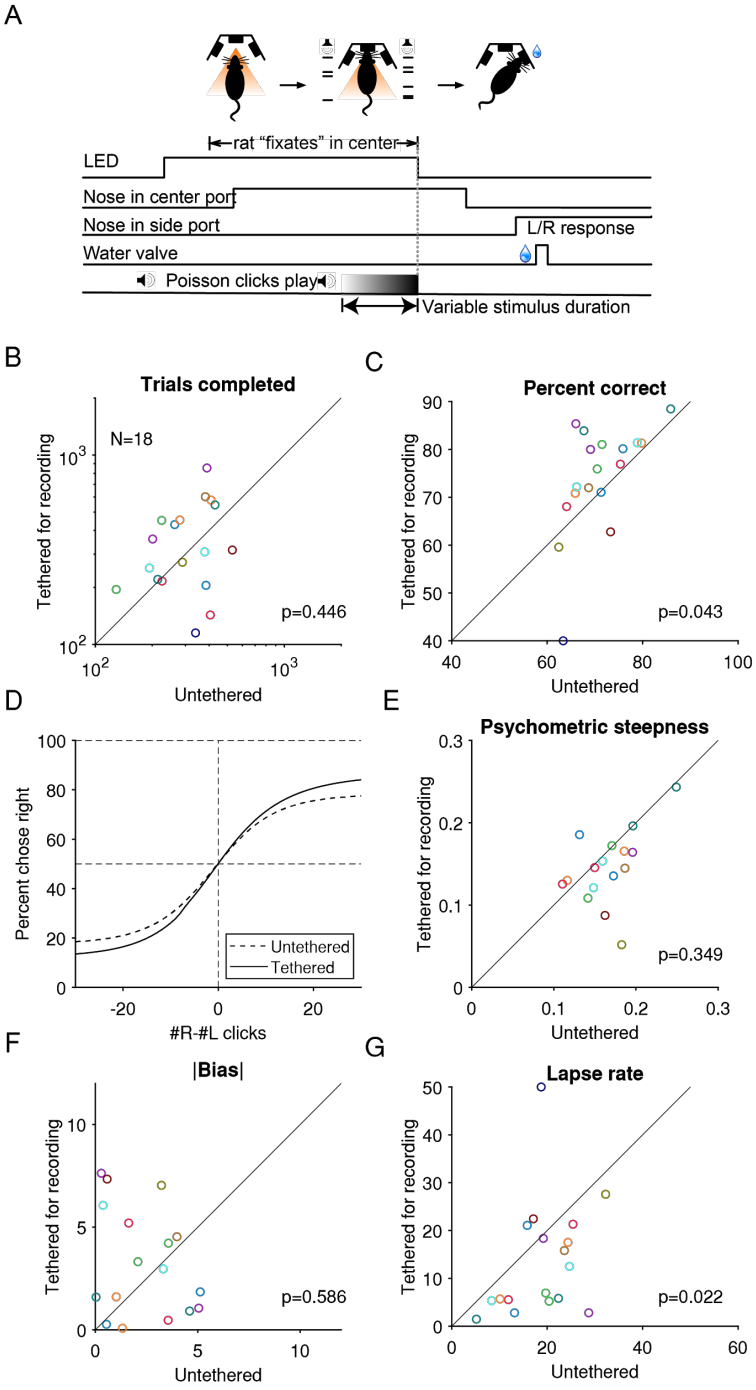


**Figure 3. While tethered for Neuropixel recording without a cable commutator, rats performed a cognitively demanding task at a level similar to when they were untethered.** A) Task schematic: rats hold their nose in the center port while listening to two concurrent streams of auditory clicks, one from a loudspeaker to its left and the other to its right. At the end of the stimulus, the rat receives a reward if it oriented toward the port on the side where more clicks were played. Adapted from (Brunton et al., 2013). B) The median number of trials completed by an animal in each training or recording session, compared between tethered and untethered. Each marker indicates an animal. P-values are based on the null hypothesis that the median difference between paired observations is zero and calculated using the Wilcoxon signed-rank test. C) The percentage of trials when an animal responded correctly. D) Logistic curves fitted to data pooled across from all animals. E) Comparison of the behavioral psychometric curves' steepness parameter (slope of the sigmoid at the inflection point). G) Absolute value of the bias parameter. F) The average of the lapse rate. A larger lapse indicates a larger fraction of trials when the animal was not guided by the stimulus or a decreased ability to take advantage of large click differences.

## Probe reuse

Previous work reported that reimplantation of two test-phase Neuropixels probes resulted in a lower event rate and signal-to-noise of detected spikes (Juavinett et al., 2019). However, event rate and signal-to-noise in the brain depend not only on probe performance but also on variability in the recording site itself. Therefore, it remains unclear to what extent probe performance degrades after prolonged implantation and explantation. Addressing this uncertainty is necessary for determining whether probe reusability is feasible.

To address this, we measured the change in the input-referred noise (i.e. noise divided by gain) in saline and compared these measurements between unimplanted and explanted probes (Methods). We first noticed that, in explanted probes, recording sites inserted into the brain showed noise amplitude (root mean squared; RMS) roughly comparable to unimplanted probes. However, the part of the shank above the brain surface tended to contain localized regions with a high fraction of noisy (>20$\mu V_{RMS}$) recording sites (Figure 4A,B). This is likely due to the application of silicone elastomer and/or petroleum jelly to those parts of the

shank during surgery, which insulated the recording sites and could not be fully removed by the enzymatic detergent used to clean the probes after explantation. These measurements may not accurately reflect performance of these recording sites upon re-implantation since insertion into the brain could remove the insulating material. Therefore, we confined further analysis to those recording sites that were lowered below the brain surface.

We compared the noise measured on the set of 2,880 recording sites from 3 new probes to the set of 3,664 recording sites from five explanted probes that had been lowered below the brain surface after their most recent explantation. We found slightly larger (0.2 μV) median RMS noise values in explanted probes (median and 95% CI: 8.30 μV and [8.23, 8.37 μV]) compared to new probes (median and 95% CI: 8.10 μV and [8.04, 8.17 μV]) (Figure 4C,D). Crucially, this small increase is roughly three orders of magnitude less than the median peak-to-peak amplitude of detected spikes (188 μV; Figure 2--supplement 2). We further examined the fraction of noisy recording sites (Figure 4E,F) and found a small (<1%) increase in the explanted probes (0.40%; 95% CI: [0.22%, 0.73%]) versus explanted probes (1.35%; [1.03%, 1.74%]).

The small magnitude of increased noise after explantation suggested probe reuse would have a negligible impact on the quality of the neural signals. Consistent with this expectation, we found comparable neural signals after three implantations of the same probe in medial frontal cortex, with no trend of increasing degradation (Figure 4G,H; ANOVA, one-way (the number of previous implants), tested on the number of SUs (*p=0.362*) and the peak-to-peak amplitude (*p=0.767*)). Analysis of neuronal encoding during the decision-making task (Figure 3A) also indicates that qualitatively similar signals were observed across implantations. Specifically, the choice selectivity averaged across units was similar between the first and third implant (Figure 4I; ANOVA, one-way (the number of previous implants), tested on the peak choice selectivity across neurons, *p=0.382*). These results indicate the minor increases in noise level across repeated cycles of implantation and explantation of the same probe did not prevent acquisition of high-quality spiking signals.

We next sought to better understand the source of the observed noise and its slight increase in explanted probes. We reasoned that the degree of correlation in noise amplitude between probe “banks” would be diagnostic. The Neuropixels probe contains fewer acquisition channels than physical recording sites, with each channel able to programmatically switch between addressing a site on bank 0 or a site on bank 1. As such, the recording sites across banks can be paired according to which acquisition channel addresses them. Noise values that are uncorrelated across these pairs presumably reflect a source intrinsic to the recording sites themselves, whereas noise values that are correlated across these pairs presumably reflect noise introduced downstream in the shared signal processing circuitry. We found that the noise across banks was highly correlated across all recording sites measured ($R^2$ = 0.89, n = 2650 recording site pairs; Figure 4J), but with significant variability in the degree of correlation among explanted probes (Figure 4K). Overall, the noise across banks was significantly higher for pairs of recording sites on new probes ($R^2$=0.94, 95% CI = [0.89,0.97], n = 1152 recording site pairs) than for those on explanted probes ($R^2$=0.84, 95% CI = [0.64,0.93], n = 1498 recording site pairs) (Figure 4L). Thus, the electrical noise in both new and explanted Neuropixels probes is mostly introduced downstream of the individual recording sites, but noise intrinsic to the recording sites plays a more significant role after long-term implantation. Taken together with the slightly larger RMS noise observed in explanted probes, these data support the idea that long-term implantation leads to modest, but measurable, degradation of the recording sites that both increases and decorrelates noise across the shank.

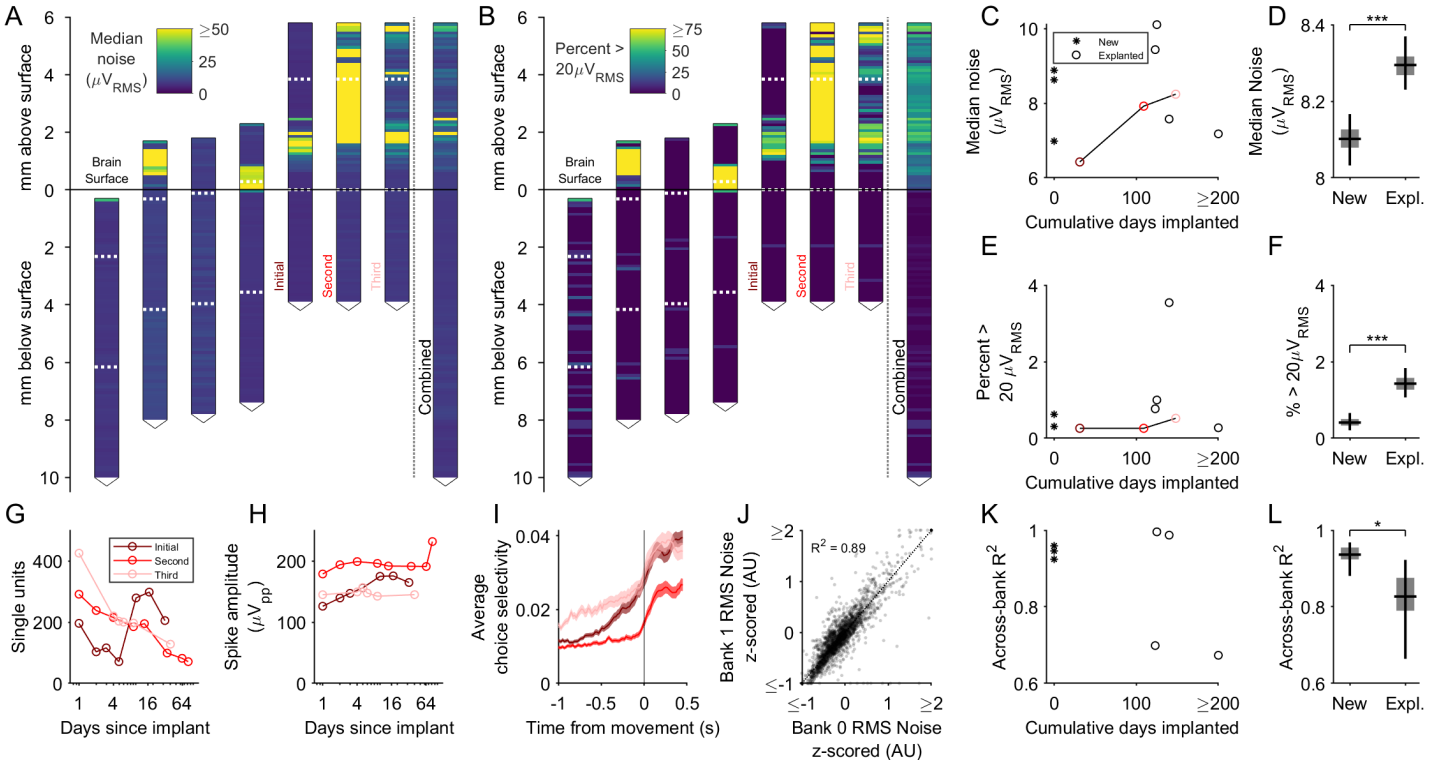


**Figure 4. Explanted probes and unimplanted probes have similar input-referred noise and can acquire neural signals of similar quality.** (A) Shank map showing the RMS input-referred noise (i.e. noise divided by gain), measured in saline, along the entire shank of explanted probes, aligned and ordered according to their implanted depth. Note high noise confined to the part of the shank above the brain surface, where silicone elastomer and/or petroleum jelly were applied during surgery. Combined data across explanted probes is at the right. Note that the three rightmost shank maps come from repeated explantations of the same probe. Dashed horizontal white lines indicate the boundaries between banks. (B) Same as A, but showing the percentage of recording sites with RMS noise >20μV. C) The median noise, shown separately by probe as a function of time implanted. Measurements from one probe that was implanted in three different animals are connected by a line. D) Box plot showing slightly higher median noise across recording sites of explanted probes compared to new probes ($p<10^{-4}$, bootstrap test for difference in median noise). Boxes and whiskers indicate the 50% and 95% bootstrap CI, respectively. Bootstrapping performed by resampling electrodes. E) The percentage of recording sites with a noise value greater than $20\mu V_{RMS}$ shown separately by probe as a function of time implanted. F) Box plot showing that the fraction of recording sites with a noise value greater than $20\mu V_{RMS}$ was slightly higher in explanted probes ($p<10^{-4}$, bootstrap test for difference in fraction of noisy electrodes). Boxes and whiskers indicate the 50% and 95% bootstrap CI, respectively. Bootstrapping performed by resampling electrodes. G-H) Signal quality of the same probe implanted in the medial frontal cortex of three separate animals. (I) Choice selectivity averaged across units did qualitatively change across successive implants. Shading indicates mean +/- 1 s.e.m. (J) Noise was highly similar across pairs of recording sites on separate banks that were addressed by the same acquisition channel (n=6,544 recording sites across new and explanted probes). Scatter plot shows RMS noise values for electrode pairs in banks 0 and 1 that were implanted below the brain surface, z-scored in groups defined by probe and bank. (K). The across-bank noise similarity ($R^2$), as computed in J, shown separately by probe as a function of time implanted. Note that the probe implanted three times is not included here, since bank 1 was never inserted into the brain. (L) Box plot showing the across-bank noise similarity ($R^2$) was lower in explanted probes (p=0.033, bootstrap test for difference in $R^2$). Boxes and whiskers indicate the 50% and 95% bootstrap CI, respectively. Bootstrapping performed by resampling electrodes.

We have provided a table detailing the outcome of all probes used in these experiments, including the probes used to develop the techniques described here (Figure 4--supplement 1). In early testing of three probes, we found that not applying petroleum jelly to the base of the chassis resulted in blood and cerebrospinal fluid entering the cavity of the 3D printed chassis and prevented retrieval of the holder. The implant of three other probes detached from the animal's skull before explantation could be attempted, but all three of these probes were used in a pilot experiment that implanted rats that had previously undergone the

injection of virus and implantation of optical fibers at least 60 days prior. All other attempted explantations were successful. Among the explanted probes, one probe could not be reused because we changed the grounding to the recording system during data acquisition, and the probe thereafter was unresponsive. All other explanted probes were reused for recording, and one was re-implanted and explanted in two additional animals (three total implants).

| Animal ID | Probe S/N | Date Implanted | Site # | Holder Version | Explantation Attempted | Reusable After Explantation |
|---|---|---|---|---|---|---|
| T176 | 619040938 | 4/6/2018 | 2 | Early | Yes, 96 days post-implant. | No [1] |
| T181 | 17131306102 | 5/24/2018 | 4 | | Yes, 536 days post-implant. | |
| T182 | 17131311881 | 5/30/2018 | | | Yes, 125 days post-implant. | Yes |
| T179 | 17131311342 | 1/20/2019 | 15 | | Yes, 176 days post-implant. | No [3] |
| T196 | 17131312042 | 4/22/2019 | 13 | | Yes, 135 days post-implant. | Yes |
| T209 | 17131311352 | 5/6/2019 | 14 | | Yes, 122 days post-implant. | Yes |
| K265 | 17131311562 | 5/16/2019 | 5 | | Yes, 53 days post-implant. | No [1] |
| A242 | 17131311621 | 5/20/2019 | 12 | | No [3] | — |
| A230 | 18005106831<br>17131308571<br>17131308411 | 7/2/2019 | 1<br>10<br>11 | Current | No [3] | — |
| T212 | 17131312432 | 8/3/2019 | 2 | | Yes, 31 days post-implant. | Yes |
| A241 | 18194823631 | 9/11/2019 | 8 | | No [3] | — |
| | 18194823302 | | 9 | | Yes, 140 days post-implant. | Yes |
| A243 | 18194824132<br>18194823211 | 9/13/2019 | 7<br>9 | | No [3] | — |
| T224 | 17131312432 | 11/14/2019 | 2 | | Yes, 81 days post-implant. | Yes |
| T219 | 18194824092 | 11/17/2019 | 6 | | No [2] | — |
| T223 | 19051017162 | 11/22/2019 | 6 | | No [2] | — |
| T249 | 17131312432 | 2/6/2020 | 2 | | Yes, 39 days post-implant. | Yes |
| A249 | 18194819132 | 2/4/2020 | 3 | | Recording ongoing. | — |
| T227 | 18194819542 | 3/14/2020 | 6 | | No [2] | — |

[1] Could not be successfully explanted, most likely because no petroleum jelly was applied at the base of the implant to mitigate blood entering into the space between the holder and the chassis and bonding them together.
[2] Implant detached before explantation could be attempted. This only occurred for rats that had undergone multiple sequential surgeries, and only after 100 days or more from the initial surgery. Skull degradation was observed in these cases.
[3] Probe was damaged during recording before explantation could be attempted.

**Figure 4--supplement 1. The outcome of all probes.** All probes that contributed to Figure 2 are included. Note that rats A230, A241, and A243 had multiple probes implanted simultaneously.

# Discussion

We sought to address several issues that have slowed widespread use of Neuropixels probes for chronic implantation in freely moving animals. First, the expected yield over multiple months is known for only a single brain area (rat medial prefrontal cortex) (Jun et al., 2017) . Second, methods currently do not exist for Neuropixels implantation that allow multiple probes to be implanted, are compatible with probe explantation, and are robust enough to ensure high yields after months on a rat or other similarly sized animal. Finally, the performance of previously explanted probes compared to unimplanted probes remains unclear. Here, inspired by previous approaches for chronic Neuropixels implants (Juavinett et al., 2019; Jun et al., 2017), we report a

system for chronic implantation of Neuropixels probes in rats that is sufficiently compact for multiple probes to be simultaneously implanted, robust enough to withstand months of implantation and hours of unmonitored recording per day, and compatible with probe recovery and reuse. We validated the system in 18 rats and documented the performance of the chronic implants over many months. Encouragingly, we found that on average, the degradation of spiking signals occurred during the first week of recording and then remained stable for up to four months. However, stability varied systematically according to brain region, with greatest stability in anterior and ventral brain regions. During recording, even with a restriction on movement imposed by a non-commutated tether, rats performed a cognitively demanding task at a level similar to their untethered performance before implantation. Lastly, we demonstrate that after multiple months of implantation, explanted probes show a decrease in performance, but of a magnitude unlikely to have a detectable consequence on acquisition of spiking signals. These results provide practical considerations that can facilitate further adoption, standardization, and development of Neuropixels probes for chronic recording in unrestrained animals.

**Holder design**

Compared to a previous design for recoverable, chronic implantation of Neuropixels probes (Juavinett et al., 2019), we aimed for different experimental goals and therefore made different design choices. A primary goal was to ensure the probe was protected from the mechanical stresses in a multi-month implant on a large rodent. For this reason, the probe was fully enclosed with a 3D printed chassis which could be strongly cemented to the skull and dampen impacts. To maximize the number of probes that can fit on a single animal, a mount for the headstage was placed on top of the probe rather than  to its side. Additionally, the cross-section of the external chassis close to its ventral face was minimized to allow probes to be inserted at a large range of angles. This change greatly facilitated multi-probe implantations. Lastly, the chassis and the holder were held together using screws rather than acrylic. One possibility this allows is to move the probe relative to the chassis to try to dissociate the probe from glial scars, though we have not tested this extensively.

Many designs of chronic implant of silicon probes or tetrodes involve a drive to move the sensor into new tissue to obtain new signals after scar tissue has accumulated (Bragin et al., 2000; J. Chung et al., 2017). We opted to not use a drivable design because we found that the recording sites above the brain often show a degradation in performance (i.e. higher input-referred noise) due to coverage by the possible combination of silicone elastomer, petroleum jelly, or dried blood or cerebrospinal fluid. Unlike tetrodes or other silicon probes, which have their recording sites at the bottom of the probe, the recording sites on the Neuropixels are along the shank. Therefore, a driveable mechanism would primarily improve signals in ventral brain areas, at the expense of signals in the dorsal areas, by driving recording sites immersed in dorsal brain regions into ventral brain areas and driving recording sites above the brain, which we observed to show signal degradation, into the dorsal areas. Because our experimental goals involve simultaneous monitoring of both ventral and dorsal brain areas, we did not choose to use a driveable design. But other experiments might benefit from a driveable design.

**Long-term stability of neural signals**

The loss of isolated units over time consisted of two components, a fast decay during the first few days after implantation, and a slower change over multiple months, yielding on average over 100 single units for at least four months. The fast component of the decline in yield was highly consistent across recording sites, while the slow component was more variable. For brain regions posterior to Bregma or within dorsal cortex, yields declined steadily until a complete loss of units after several months. The rate of this steady decline also depended on shank orientation. However, we could not detect an effect of the position of an electrode on the probe shank, despite our prediction that greater flexibility of the shank toward its tip would reduce long-term tissue damage of the surrounding tissue. These observations suggest that the recording of dorsal cortex and posterior brain area may benefit from other refinements to techniques for chronic implantation.

Given the excellent performance of the probes upon reimplantation and dependence of yield on anatomical location, the decrease in yield must be related to changes in the neural tissue, changes which in

turn must be heterogeneous across brain areas. Implantation of a chronic neural probe initiates a cascade of biochemical reactions that are part of the wound healing process. This has been divided into an acute and chronic phase (Gulino et al., 2019). The acute phase, lasting days or weeks, is caused by the trauma associated with the removal of the skull and meninges and insertion of a probe which ruptures the blood-brain barrier. These injuries lead to rapid neuronal cell death due to oxidative stress and activate a neuroinflammatory response mediated by glia (Saxena et al., 2013). This is followed by a chronic phase, lasting months or years, characterized by a further immune response and eventually the encapsulation of the probe by a glial scar.

Several features of our data suggest that neuronal cell death during the acute phase of the tissue response is likely the primary cause of the decrease in yield. First, most of the loss in yield occurred during the first week, before encapsulation is thought to occur (Wellman & Kozai, 2017). Second, the loss consisted primarily of a loss of isolated units, with no decrease in average spike amplitude. This suggests the loss of units both near and far from the shank, and no overall change in the conductivity of the surrounding tissue. This would be consistent with neuronal cell death but not with insulation of the probe in scar tissue.

We also observed pronounced differences in yield decline after this initial period depending on the electrode's AP position and on whether it was in dorsal cortex. To our knowledge these findings cannot be easily explained based on the current literature. One potential mechanism is variability in the degree of ongoing injury after implantation due to motion of the brain relative to the skull (and therefore to a rigid probe anchored to the skull). The relative displacement could be particularly acute during head acceleration (Zhou et al., 2020), although even respiration causes some degree of micromotion, and both of these types of relative motion have been directly implicated in glial activation (Lind et al., 2013; Muthuswamy et al., 2005). Relative motion is expected to be variable across brain areas for at least two reasons. First, the amount of brain micromotion around an implant increases upon a durotomy (Muthuswamy et al., 2005). This may contribute to the loss of units in superficial cortex relative to deeper structures. Second, the degree of micromotion and the response of the brain to deformation and inertial forces is heterogeneous ((MacManus et al., 2018)(Sloots et al., 2020); (Bayly et al., 2005), (Budday et al., 2015), (Jacobo et al., 2014). The studies that have examined this have primarily sought to explain the heterogeneous effects of traumatic brain injury, so their implications for the long-term response to a chronically implanted foreign body are unclear. Nonetheless, these studies demonstrate clear heterogeneity in the mechanical properties of the brain, that may underlie differences in yield that can be expected after chronic implantation of rigid probes. For this reason, future probe designs that allow for greater mechanical flexibility may be essential for maintaining high-yield recordings in some brain structures over long periods of time ((J. E. Chung et al., 2019; Jeong et al., 2015; Kim et al., 2004; Luan et al., 2017; Polikov et al., 2005).

**Model interpretation and limitations**

A plausible model of the loss of neurons over time is necessary for statistical inference on experimental factors that affect chronic stability of neural implants, but this has not been done before. We found that a single-term exponential regression model performed far worse at fitting the data compared to a model with two exponential terms. The success of the sum-of-exponentials model would be consistent with two distinct subpopulations of neurons having different rates of decay. One subpopulation disappears at a fast rate that is potentially due to acute damage during the probe insertion (Bjornsson et al., 2006). The other subpopulation declines at a slower rate, consistent with the chronic tissue response and ongoing damage from tissue motion or acceleration relative to the probe. The model fits indicated that the experimental factors had little effect on fast-decaying subpopulation.

However, we have no direct evidence that there are in fact two distinct subpopulations. It is possible that a model that supposes a dynamic decay rate—a qualitatively distinct account of the loss over time—fit the data here as well, if not better. Adjudicating which account is more reliable would likely require not only model comparison but direct experimental testing. The supposition of distinct subpopulation with different change rates predicts that the neurons that decayed rapidly suffered greater damage from the implantation. One

possible experiment is to track neurons across days and examine whether neurons that survived longer are those that showed fewer signs of damage in their activity, such as bursting activity, immediately after implantation.

### Performance of Explanted Probes

Measurements in saline of explanted probes revealed that recording sites that had been lowered into the brain showed only a very small increase in noise relative to unimplanted probes. This difference was much too small to impair high-quality chronic recordings, which we confirmed with multiple cycles of implantation and explantation. By contrast, the part of the probe that remained above the brain surface exhibited local regions with very high noise. This is presumably related to the application of silicone elastomer and/or petroleum jelly to the exposed part of the shank during surgery, which may not have been fully removed after cleaning with an enzymatic detergent.

First and foremost, these findings support the conclusion that Neuropixels probes, used with the system outlined here, are able to withstand months of implantation in neural tissue followed by explantation, with negligible reduction in performance of the recording sites lowered into the brain. As for the superficial recording sites, it is difficult to know whether the high noise observed on many probes would impair neural data acquisition upon re-implantation, as the corrosive environment of the brain may dissolve any insulating materials applied in a previous surgery. Supporting this possibility, the noise was highly variable on the superficial electrodes of a probe explanted three times, suggesting that these measurements do not reflect a permanent degradation. Nonetheless, we conclude that it may be wise to lower as many recording sites into the brain as possible during surgery, to shield the superficial electrodes from materials applied in surgery that may be difficult to remove. In addition, identifying cleaning reagents that are compatible with Neuropixels probes and specifically designed to remove non-biological materials such as silicone would be useful.

Finally, we observed a high degree of correlation in the noise amplitude measured across distant pairs of recording sites that were addressed by the same acquisition channel. This implicates the signal processing circuitry as the major source of noise in the probes, rather than the recording sites themselves. Because this circuitry is not exposed to brain tissue, this bodes well for the long-term performance of the probes, consistent with our empirical findings. Nonetheless, we did observe a slight decrease in the degree of correlation across banks in explanted probes. Taken together with the slight increase in noise amplitude, this points to a modest degradation of the recording sites after long-term implantation.

### Conclusion

Chronic implantation of microelectrodes has been and will likely continue to be an essential technique in neuroscience. However, the Neuropixels probe—a major advance in the electrophysiological toolkit—has not yet reached its full potential due to technical obstacles associated with long-term chronic implantation. The system described here represents a significant step forward in overcoming these obstacles and achieving highly stable, cost-effective, and parallel recordings from chronically implanted Neuropixels probes in freely moving animals. Our characterization of this system may also serve to inform future development of new electrophysiological probes for chronic use as well as improve implantation methods for species and experimental questions not considered here.

## Methods

### Subjects

A total of 18 male Long-Evans rats (*Rattus norvegicus*) were used in this study. Four of them were BAC transgenic rats expressing Cre recombinase. These rats were used for the purpose of targeting optogenetic constructs to cell types of interest for experiments not described in the present report. These rats came from the following three lines: LE-Tg(Pvalb-iCre)2Ottc (n=1), LE-Tg(Gad1-iCre)3Ottc (n=2), LE-Tg(Drd2-iCre)1Ottc

(n=1). These lines were made by the Transgenic Rat Project at the National Institute of Drug Abuse (NIDA) and were obtained from the Rat Resource and Research Center (RRRC) at the University of Missouri.

All rats were water restricted to motivate them to work for water as reward, and obtained a minimum volume of water per day equal to 3% of their body mass. If rats consumed less than this minimum during performance of the task, additional water was offered after training. Rats were kept on a reversed 12-hr light-dark cycle and were trained in their dark cycle. Rats were pair housed whenever possible during early training, but were always single housed after implantation to prevent damage to the implant. Starting from the day before each surgery to at least three days after the surgery, rats were given ab lib access to water. Animal use procedures were approved by the Princeton University Institutional Animal Care and Use Committee and carried out in accordance with National Institute of Health standards.

**Implant Construction**

The probes used were commercially available Neuropixels 1.0 probes (IMEC, Leuven, Belgium), with the option of a flat silicon spacer attached parallel to the plane of the probe, except for one (among 20), which was phase 3A option 1 probe. A protocol for constructing the implant is available, with photographs illustrating each step, at https://github.com/Brody-Lab/chronic_neuropixels. We summarize these procedures here. First, to prepare a probe for implantation, the silicon spacer was glued to a 3D-printed plastic base with dovetail rails, inspired by the stainless steel dovetail adapter now optionally shipped on the probes. This dovetail connection mated with matching dovetail rails on an internal holder that could be manipulated using a stereotaxic holder (Kopf, Tujunga, CA, USA; Model 1766-AP Cannula Holder). The gold pads on the probe flex cable corresponding to ground and external reference were shorted by soldering a 0.01” silver wire to them. The entire apparatus was then enclosed with a 3D-printed external chassis and the holder and the chassis were connected using screws. The chassis was then wrapped in conductive tape to provide electromagnetic shielding and coated in a thin layer of C&B Metabond (Parkell, Edgewood, NY, USA) for better adherence to the dental acrylic during implantation. The bottom surface of the chassis was sealed with petroleum jelly, dispensed in liquid droplets from a low-temperature cautery (Bovie), to prevent blood from entering the chassis after implantation. During the surgery, after the probe was inserted into the brain, the chassis, but not the holder, was fixed to the skull surface using adhesive cement and acrylic. The internal holder did not come into contact with the adhesives and therefore can be detached from the chassis by removal of the screws.

During recording, a 3D-printed “headstage-mount” mated directly with the chassis through a latching mechanism, and mounted headstages were connected to the flex cable of a probe. Up to four headstages can be mounted so that up to four probes can be simultaneously implanted and recorded using this system. (Although, note that the size and geometry of the implant places constraints on the set of coordinates that can be simultaneously targeted, constraints that become more significant when more probes are implanted at once). The recording cables were placed inside a corrugated plastic sleeving to avoid small bending radiuses (1/2” internal diameter, McMaster 7840K73). This sleeving was permanently attached to the recording cap using electrical tape.

All parts except the probe itself and the screws were 3D printed in-house using Formlabs SLA printers (Form 2 and Form 3). Prints used standard black Formlabs resin, except for the recording cap which was printed in “Tough” Formlabs resin, required for the flexible latching mechanism.

A subset of implants (n=7) were made using an earlier version of the 3D design that embodied a similar design principle but were slightly larger in size. Results were similar between the two versions of the design and were therefore combined.

CAD files, detailed protocols for implant assembly and surgeries, code, and data are provided at https://github.com/Brody-Lab/chronic_neuropixels.

**Implantation**

Surgeries were performed using techniques that were similar to those reported previously (Erlich et al., 2011). Rats were placed in an induction chamber under 4% isoflurane for several minutes to induce anesthesia

and then injected with 10 mg ketamine and 6µg buprenorphine intraperitoneally to further assist induction and provide analgesia. Rats were then placed on a stereotaxic frame (Kopf Instruments) and anesthesia was maintained with 1-2% isoflurane flowing continuously through a nose cone. After verifying surgical levels of anesthesia, rats were secured in ear bars, shaved and cleaned with ethanol and betadine. A midline incision was then made with a scalpel and a spatula was used to clean the skull of all overlying tissue.

A small, crater-like craniotomy roughly 1mm in diameter was made at the site of probe implantation. A needle was used to cut an approximately 0.5 mm slit in the dura into which the probe was later lowered. This procedure was repeated at the site of each probe to be implanted. Next, a craniotomy and durotomy were performed at a site distal to the brain region(s) to be recorded, typically in the olfactory bulb or cerebellum, into which a ground (wire, pin, or cannula) would later be inserted. Saline soaked Gelfoam (Pfizer Injectables) was placed in the craniotomies to protect the brain while a thin coat of C&B Metabond (Parkell, Inc) was applied to the skull surface. Then, the Gelfoam was removed from the ground craniotomy and the ground was lowered into the brain. This craniotomy was then sealed with Kwik-Sil (WPI) and the ground was fixed in place using a small amount of dental composite (Absolute Dentin, Parkell, Inc.).

Gelfoam was removed one by one from the remaining craniotomies and the probes inserted. Probes were manually lowered at a rate of 0.1 mm every 10-30 s. After a probe was fully inserted, a small quantity (<5uL) of soft silicone gel (DOWSIL 3-4680, Dow Chemical) was injected to seal the craniotomy. We found that harder silicones, such as Kwik-Sil (WPI), could damage the probe shank upon application. Dental composite (Absolute Dentin, Parkell) was then used to create a wall-like barrier covering the gaps below the four ventral edges of the external chassis and the skull, creating a seal around the probe shank. After these steps were completed for each probe, the silver wires soldered to the ground and external reference pads on each probe flex cable were then soldered to the common animal ground. Acrylic resin (DuraLay, Reliance Dental) was applied to secure the entire implant assembly to the Metabond-coated skull. Rats were given ketoprofen after the surgery and again 24 and 48 hours post-operative and recovered with ad lib access to water for 5 days before returning to water restriction.

**List of Implantation Sites**

The table below details the coordinates of each probe insertion site, relative to Bregma. The AP position is positive for sites anterior to Bregma. A positive angle in the coronal plane indicates that the probe tip was more lateral than the insertion site at the brain surface, and a positive angle in the sagittal plane indicates that the probe tip was more anterior than the insertion site.

| Site # | AP (mm) | ML (mm) | Depth (mm) | Angle in the coronal plane (°) | Angle in the sagittal plane (°) | Brain regions | No. Implanted probes |
|---|---|---|---|---|---|---|---|
| 1 | 4.0 | 0.5 | 7.5 | 26 | -29 | Secondary motor cortex, dorsomedial striatum, globus pallidus | 1 |
| 2 | 4.0 | 1.0 | 4.2 | -10 | 0 | Medial frontal cortex (secondary motor cortex, cingulate cortex, medial prefrontal cortex (prelimbic and medial orbital cortices)) | 4 |
| 3 | 2.2 | 2.1 | 6.8 | -5 | 0 | Secondary motor cortex, anterior dorsal striatum, anterior ventral striatum | 1 |
| 4 | 1.9 | 1.3 | 8.2 | 15 | 0 | | 2 |
| 5 | 1.9 | 0.8 | 7 | 20 | 0 | | 1 |
| 6 | 0.0 | 2.4 | 7.9 | 0 | 15 | | 3 |
| 7 | 0.7 | 2.45 | 9 | 0 | 0 | Preoptic area, amygdala, ventral pallidum, globus pallidus, dorsomedial striatum, motor cortex | 1 |
| 8 | 0.7 | 2.15 | 10 | 2 | 0 | Preoptic area, bed nucleus of the stria terminalis, dorsomedial striatum, motor cortex | 1 |
| 9 | -0.6 | 4.0 | 10 | -2 | 0 | Somatosensory cortex, posterior dorsomedial striatum, amygdala | 1 |
| 10 | -0.8 | 4.0 | 6.6 | -2 | 0 | Somatosensory cortex, dorsomedial striatum | 1 |
| 11 | -2.2 | 5.0 | 8.6 | 5 | 0 | Somatosensory cortex, striatum tail, amygdala, piriform cortex | 1 |
| 12 | -2.35 | 4.95 | 7.6 | 5 | 5 | Somatosensory cortex, striatum tail, amygdala | 1 |
| 13 | -6.6 | 1.6 | 7.8 | -40 | 0 | Primary visual cortex, retrosplenial cortex, superior colliculus, and inferior colliculus | 1 |
| 14 | -6.8 | 1.7 | 8 | -40 | 0 | | 1 |
| 15 | -7.0 | 3.0 | 5.8 | 0 | 0 | Primary visual cortex, postrhinal cortex, and inferior colliculus | 1 |

**Explantation**

To explant a probe, the animal was first anesthetized and placed in the stereotaxic frame. Then, a stereotaxic arm was attached to the probe's internal holder and the screws fixing the internal holder and external chassis were removed. The stereotaxic arm was raised until the internal holder, carrying the probe, was fully removed. The internal holder sometimes adhered to the external chassis after screw removal. In these cases, the external chassis was carefully drilled away with a dental drill until the internal holder could be easily removed. After explantation, the probe shank was fully immersed in 1% tergazyme (Alconox) for 24-48h, followed by a brief rinse in distilled water and isopropyl alcohol, in that order.

**Electrophysiological recordings**

Electrophysiological recordings were performed using either commercially available Neuropixels 1.0 acquisition hardware (Putzeys et al., 2019) or earlier test-phase IMEC acquisition hardware. The former was used in conjunction with PCI eXtensions for Instrumentation (PXI) hardware from National Instruments (including a PXIe-1071 chassis and PXI-6133 I/O module for recording analog and digital inputs.) We used SpikeGLX software (http://billkarsh.github.io/SpikeGLX/) to acquire the data. For measurement of signal stability over time, the selected reference was a silver wire shorted to the ground wire and penetrating the brain at a different location from the probe insertion site. The amplifier gain used during recording was 500. The recording channels addressed either the deepest 384 recording sites ("bank 0") or the second deepest 384 recording sites ("bank 1"), and recordings lasted approximately ten minutes. Recordings were made on days with logarithmically-spaced intervals.

Spikes were sorted offline using Kilosort2 (Pachitariu, 2020), using default parameters and without manual curation. A unit was considered a single-unit if Kilosort2 categorized that unit as "good." A putative single unit meets both of the following conditions: 1) the proportion of refractory violations was less than 0.05. This proportion was computed by calculating a unit's autocorrelogram in one millisecond bins, summing the values in the central bins, and normalizing the sum by the expected sum from the mean firing rates. This normalized value was compared to a normalized sum similarly calculated from the shoulder of the autocorrelogram. The span of the central bins range varied from +/-1.5 ms to +/-10.5 ms, and a separate ratio was computed for each span. The span of the shoulder bins were either +/-10.5 ms to +/-50 ms or +/-25.5 ms to +/-499.5 ms. A separate ratio was calculated for each combination central bin span and shoulder bin span. The minimum ratio across combinations was the proportion of refractory violations. 2) For each span of central bins, a probability was calculated for the number observed coincidences in the central bins of the autocorrelogram, or fewer, being produced by a Poisson distribution with observed mean firing rate of the unit. The minimum probability across spans of central bins has to be less than 0.05.

**Sum-of-exponentials model**

In Figure 2D-L and Figure 2--supplement 3, the number of units recorded from each session was modelled as a sum of two exponential decay terms:

$$N = N_1(\alpha e^{k_{fast}(t-1)} + (1-\alpha)e^{k_{slow}(t-1)}) + \varepsilon \quad (1)$$

$N$ is the number of units (or SUs), $N_1$ is the number units on the first day after implant, $t$ is the number of days after the implantation, $\alpha$ indicates the fraction of the units that are rapidly decaying with the change rate $k_{fast}$, and the remaining fraction ($1-\alpha$) decays with a slower (less negative) time constant $k_{slow}$, and, $\varepsilon \sim N(0, \sigma^2)$. The estimated parameters were found by maximizing the log-likelihood using MATLAB's *fmincon* function, using the interior-point algorithm, and with the constraints that $-10 < k_{fast} \leq k_{slow} < -10^{-6}$. The exponential terms at these bounds are effectively 0 or 1, and the bounds were imposed to improve the consistency of the fitting. Error in the coefficient estimates was estimated as using the percentile bootstrap confidence intervals computed from 1000 bootstrap samples.

In Figure 2M-P, the sum-of-exponentials model was fit to the number of units recorded from each electrode from each recording session:

$$N = Poiss(\lambda) \quad (2)$$

$$\lambda = N_1[\alpha e^{k_{fast}(t-1)} + (1-\alpha)e^{k_{slow}(t-1)}] \quad (3)$$

$$N_1 = \beta_0^{N_1} + \beta_{AP}^{N_1} AP + \beta_{DV}^{N_1} DV + \beta_{DV>-2}^{N_1} DV_{>-2} + \beta_{ML}^{N_1} ML \quad (4)$$

$$k_{fast} = \beta_{fast} + k \quad (5)$$

$$k_{slow} = \beta_{slow} + k \quad (6)$$

$$k = \beta^k_{AP} AP + \beta^k_{DV} DV + \beta^k_{DV>-2} DV_{DV>-2} + \beta^k_{ML} ML + \beta^k_{SP} SP + \beta^k_{SO} SO \quad (7)$$

The number of units recorded on an individual electrode during a session ($N$) depends on the unit count on the first day after implant ($N_1$), a weighted sum of the regressors $AP$ (mm anterior), $DV$ (mm brain surface), $DV>-2$ (1 if the electrode has a *DV* position greater than -2, which is approximately dorsal cerebral cortex, and 0 otherwise), and $ML$ (mm from midline), plus a constant term. In variants of the model that are not shown, we also included regressors that were categorical variables along the AP or ML axis, but those regressors were consistently excluded by the parameter selection process (see below).The model supposes two distinct subpopulations with different rates of exponential change. A fraction of units ($\alpha$) changes exponentially at the rate of $k_{fast}$, and the remaining fraction of units ($1-\alpha$) changes at the rate of $k_{slow}$. The decay rates of both subpopulations depend on a weighted sum of the regressors $AP$, $DV$, $DV>-2$, $ML$, $SP$ (mm from the tip of the probe shank), and $SO$ (shank orientation, whether the plane of the shank is parallel to the brain's coronal, as opposed to sagittal, plane), as well as a constant term.

Because the regressors are partly correlated, the estimate of the coefficient of each regressor, as well as the error of the estimate, depend on what other regressors are included in the model. To make the inference more reliable, we first selected the subset of regressors that allowed the model to best predict unit count over time. During all-subset variable selection, model variants included either the continuous regressor $DV$ or the categorical $DV>-2mm$, but not both. The number of model variants were 448 ($2^{10}$ - 576 subsets with both the $DV$ and $DV>-2$ regressors in either the $N_1$ or $k$ term). In addition to the regressors related to the experimental factors, all model variants included the variables $\alpha$, $k_{fast}$, $k_{slow}$, a constant in $N_1$.

The model was fitted by maximizing log-likelihood using MATLAB's *fmincon* function, with the constraint that $-10 < k_{fast} \leq k_{slow} < -10^{-6}$. Because the estimate of the coefficient of each regressor depends on whether other regressors are included in the model, variable selection was first performed before performing coefficient inference. All subsets of the variables were fit in different model variants and evaluated using out-of-sample log-likelihood (LL) computed using five-fold cross-validation. To avoid underestimating the confidence intervals, the data was randomly divided in halves, separately used for variable selection and for estimating the error of coefficient estimates. The procedure of randomly splitting the data, selecting the best model using one half of the data, and using the other half to estimate the coefficients was repeated ten times to confirm that the results were consistent. The point and error estimates of the coefficients shown in Figure 2M-P were from the repetition in which the best model's out-of-sample LL was the median across the ten repetitions. Error in the coefficient estimates were 95% percentile bootstrap confidence intervals calculated from 1,000 bootstrap samples.

Conclusions were not changed if a Gaussian-noise model were used. A single-term exponential model was associated with much lower out-of-sample log-likelihood and therefore not used. The all-subset variable selection procedure was preferred over stepwise selection due to its greater consistency in model selection, and it was used instead of LASSO because it allows comparison between the best model and the runner-up models.

**Behavioral task**

Training took place in an operant box with three nose ports (left, center and right) and two speakers, placed above the right and left nose ports. Each trial began with a visible light-emitting diode (LED) turning on in the center port. This cued the rat to insert its nose into the center port and keep it there until the LED was turned off (1.5 s "fixation" period). In each trial, rats were concurrently presented with two trains of auditory pulses, one train from a loudspeaker on its left, and the other from a loudspeaker on its right (Brunton et al.,

2013). At the end of each trial, the subjects received a reward if they oriented to the port on the side of the auditory train with the greater total number of pulses. The timing of pulses varied both within and across individual trials and between the left and right streams. Behavioral control and stimulus generation used Bcontrol software (brodylabwiki.princeton.edu/bcontrol). Before probe implantation, subjects were trained in a semi-automated, high-throughput training facility, each in a behavioral enclosure 13" wide, 11" deep and 18.5" tall within a sound-attenuated chamber (Coulbourn, Holliston, MA, USA). After surgery, tethered behavioral performance took place in a larger behavioral enclosure that was 13" wide, 11" deep and 40" tall within a sound-attenuated chamber and built-in Faraday cage (IAC, Naperville, IL, USA). Untethered performance took place in the training facility, as before surgery.

**Behavioral performance metrics**

The performance of each rat (pooled across multiple sessions) was fit with a four-parameter logistic function:

$$P(right) = \gamma 0 + \gamma 1/(1 + exp(-\beta(x - \alpha))$$

where *x* is the click difference on each trial (number of right clicks minus number of left clicks), and *P(right)* is the fraction of trials when the animal chose right. The parameter α is x value (click difference) at the inflection point of the sigmoid, quantifying the animal's bias; β is the slope of the sigmoid at x = α, quantifying the sensitivity of the animal's choice to the stimulus; $\gamma 0$ is the minimum *P(right)*; and $\gamma 0+\gamma 1$ is the maximum *P(right)*. The lapse rate is $(1-\gamma 1)/2$. The number of trials completed excludes trials when the animal prematurely broke fixation and trials after the animal in which the animal failed to choose a side port after five seconds.

**Measurement of input-referred noise**

The RMS noise of the AP band (300Hz - 10kHz) of each recording site was measured in a 0.9% phosphate buffered saline (PBS) solution, following the procedure described in the Neuropixels User Manual (IMEC). To accurately compare across recording sites and probes, this procedure requires first determining a gain correction factor for each recording site, so that the nominal and actual gains match. To do this, we measured the response to a 4mVpp, 1.8kHz sine wave generated using an arbitrary waveform generator (PXIe-5413, National Instruments) in 0.9% PBS. We compared the measured amplitudes on each recording site to the amplitude measured on an independent, calibrated I/O module (PXI-6133, National Instruments) to determine the gain correction factor.

**Choice selectivity**

This metric is based on the receiver operating characteristic (ROC) and indexes how well an ideal observer can classify left- versus right-choice trials using the spike counts of an isolated unit. Spikes were counted in 0.1 s bins stepped in 0.02 s, from 1 s before movement onset to 0.5 s afterwards. Trials were included for analysis if the rat did not prematurely disengage from the center port and also reported its choice within five seconds after it was cued to do so. An ROC curve classifying left- and right-choice trials was constructed based on the spike counts of each unit in each time bin. The area under the ROC curve ranged from 0 to 1, with values greater than 0.5 indicating a larger mean spike count associated with right-choice trials. Because the present analysis concerns only the magnitude and not the directionality of the choice selectivity, a value *x* less than 0.5 was flipped to the corresponding value above 0.5, i.e. |x-0.5| + 0.5. The choice selectivity results were from the first recording session for each animal after the implantation when the animal had completed more than a hundred trials (4-11 days after surgery).

## Author contributions

AGB, DG, and TZL designed the experiments. AGB, CDK, DG, TZL, and VAE collected the data. AGB, TZL, and VAE analyzed the data. AGB, CDB, and TZL wrote the manuscript.

## Acknowledgements

We thank T. Harris, M. Oostland, and M. Schottdorf for comments and discussion; J. Teran for technical assistance; J. Putzeys for advice on measurement of input-referred noise; and J. Colonell and B. Karsh for advice on the recording equipment.

## References

Allen, W. E., Chen, M. Z., Pichamoorthy, N., Tien, R. H., Pachitariu, M., Luo, L., & Deisseroth, K. (2019). Thirst regulates motivated behavior through modulation of brainwide neural population dynamics. *Science*, *364*(6437), 253.

Bayly, P. V., Cohen, T. S., Leister, E. P., Ajo, D., Leuthardt, E. C., & Genin, G. M. (2005). Deformation of the human brain induced by mild acceleration. *Journal of Neurotrauma*, *22*(8), 845–856.

Bjornsson, C. S., Oh, S. J., Al-Kofahi, Y. A., Lim, Y. J., Smith, K. L., Turner, J. N., De, S., Roysam, B., Shain, W., & Kim, S. J. (2006). Effects of insertion conditions on tissue strain and vascular damage during neuroprosthetic device insertion. *Journal of Neural Engineering*, *3*(3), 196–207.

Bragin, A., Hetke, J., Wilson, C. L., Anderson, D. J., Engel, J., Jr, & Buzsáki, G. (2000). Multiple site silicon-based probes for chronic recordings in freely moving rats: implantation, recording and histological verification. *Journal of Neuroscience Methods*, *98*(1), 77–82.

Brunton, B. W., Botvinick, M. M., & Brody, C. D. (2013). Rats and humans can optimally accumulate evidence for decision-making. *Science*, *340*(6128), 95–98.

Budday, S., Nay, R., de Rooij, R., Steinmann, P., Wyrobek, T., Ovaert, T. C., & Kuhl, E. (2015). Mechanical properties of gray and white matter brain tissue by indentation. *Journal of the Mechanical Behavior of Biomedical Materials*, *46*, 318–330.

Chung, J. E., Joo, H. R., Fan, J. L., Liu, D. F., Barnett, A. H., Chen, S., Geaghan-Breiner, C., Karlsson, M. P., Karlsson, M., Lee, K. Y., Liang, H., Magland, J. F., Pebbles, J. A., Tooker, A. C., Greengard, L. F., Tolosa, V. M., & Frank, L. M. (2019). High-density, long-lasting, and multi-region electrophysiological recordings using polymer electrode arrays. *Neuron*, *101*(1), 21–31.e5.

Chung, J., Sharif, F., Jung, D., Kim, S., & Royer, S. (2017). Micro-drive and headgear for chronic implant and recovery of optoelectronic probes. *Scientific Reports*, *7*(1), 2773.

Davidson, J. D., & El Hady, A. (2019). Foraging as an evidence accumulation process. *PLoS Computational Biology*, *15*(7), e1007060.

Erlich, J. C., Bialek, M., & Brody, C. D. (2011). A cortical substrate for memory-guided orienting in the rat. *Neuron*, *72*(2), 330–343.

Erö, C., Gewaltig, M.-O., Keller, D., & Markram, H. (2018). A cell atlas for the mouse brain. *Frontiers in Neuroinformatics*, *12*, 84.

Gulino, M., Kim, D., Pané, S., Santos, S. D., & Pêgo, A. P. (2019). Tissue response to neural implants: the use of model systems toward new design solutions of implantable microelectrodes. *Frontiers in Neuroscience*, *13*, 689.

Harris, K. D., Henze, D. a., Csicsvari, J., Hirase, H., & Buzsáki, G. (2000). Accuracy of tetrode spike separation as determined by simultaneous intracellular and extracellular measurements. *Journal of Neurophysiology*, *84*(1), 401–414.

Hoy, J. L., Bishop, H. I., & Niell, C. M. (2019). Defined cell types in superior colliculus make distinct contributions to prey capture behavior in the mouse. *Current Biology: CB*, *29*(23), 4130–4138.e5.

Ito, H. T., Zhang, S.-J., Witter, M. P., Moser, E. I., & Moser, M.-B. (2015). A prefrontal-thalamo-hippocampal circuit for goal-directed spatial navigation. *Nature*, *522*(7554), 50–55.

Jacobo, A.-M., Johan, D., Marten, R., Ejima, S., & Koshiro, O. (2014). Validation of local brain kinematics of a novel rat brain finite element model under rotational acceleration. *International Journal of Automotive Engineering*, *5*(1), 31–37.

Jeong, J.-W., Shin, G., Park, S. I., Yu, K. J., Xu, L., & Rogers, J. A. (2015). Soft materials in neuroengineering for hard problems in neuroscience. *Neuron*, *86*(1), 175–186.

Juavinett, A. L., Bekheet, G., & Churchland, A. K. (2019). Chronically implanted Neuropixels probes enable high-yield recordings in freely moving mice. *eLife*, *8*. https://doi.org/10.7554/eLife.47188

Jun, J. J., Steinmetz, N. A., Siegle, J. H., Denman, D. J., Bauza, M., Barbarits, B., Lee, A. K., Anastassiou, C. A., Andrei, A., Aydın, Ç., Barbic, M., Blanche, T. J., Bonin, V., Couto, J., Dutta, B., Gratiy, S. L., Gutnisky, D. A., Häusser, M., Karsh, B., … Harris, T. D. (2017). Fully integrated silicon probes for high-density recording of neural activity. *Nature*, *551*(7679), 232–236.

Kim, Y.-T., Hitchcock, R. W., Bridge, M. J., & Tresco, P. A. (2004). Chronic response of adult rat brain tissue to implants anchored to the skull. *Biomaterials*, *25*(12), 2229–2237.

Krupic, J., Bauza, M., Burton, S., & O'Keefe, J. (2018). Local transformations of the hippocampal cognitive map. *Science*, *359*(6380), 1143–1146.

Lecomte, A., Descamps, E., & Bergaud, C. (2018). A review on mechanical considerations for chronically-implanted neural probes. *Journal of Neural Engineering*, *15*(3), 031001.

Lind, G., Linsmeier, C. E., & Schouenborg, J. (2013). The density difference between tissue and neural probes is a key factor for glial scarring. *Scientific Reports*, *3*, 2942.

Luan, L., Wei, X., Zhao, Z., Siegel, J. J., Potnis, O., Tuppen, C. A., Lin, S., Kazmi, S., Fowler, R. A., Holloway, S., Dunn, A. K., Chitwood, R. A., & Xie, C. (2017). Ultraflexible nanoelectronic probes form reliable, glial scar-free neural integration. *Science Advances*, *3*(2), e1601966.

MacManus, D. B., Pierrat, B., Murphy, J. G., & Gilchrist, M. D. (2018). Region and species dependent mechanical properties of adolescent and young adult brain tissue. *Scientific Reports*, *8*(1), 11234.

Mora Lopez, C., Putzeys, J., Raducanu, B. C., Ballini, M., Wang, S., Andrei, A., Rochus, V., Vandebriel, R., Severi, S., Van Hoof, C., Musa, S., Van Helleputte, N., Yazicioglu, R. F., & Mitra, S. (2017). A Neural Probe With Up to 966 Electrodes and Up to 384 Configurable Channels in 0.13 µm SOI CMOS. *IEEE Transactions on Biomedical Circuits and Systems*, *11*(3), 510–522.

Muthuswamy, J., Saha, R., & Gilletti, A. (2005). Tissue micromotion induced stress around brain implants. *2005 3rd IEEE/EMBS Special Topic Conference on Microtechnology in Medicine and Biology*, 102–103.

Pachitariu, M. (2020). *MouseLand/Kilosort2: release for Zenodo DOI*. https://doi.org/10.5281/zenodo.3597475

Paxinos, G., & Watson, C. (2006). *The Rat Brain in Stereotaxic Coordinates:* Elsevier.

Polikov, V. S., Tresco, P. A., & Reichert, W. M. (2005). Response of brain tissue to chronically implanted neural electrodes. *Journal of Neuroscience Methods*, *148*(1), 1–18.

Putzeys, J., Raducanu, B. C., Carton, A., De Ceulaer, J., Karsh, B., Siegle, J. H., Van Helleputte, N., Harris, T. D., Dutta, B., Musa, S., & Mora Lopez, C. (2019). Neuropixels data-acquisition system: a scalable platform for parallel recording of 10 000+ electrophysiological signals. *IEEE Transactions on Biomedical Circuits and Systems*, *13*(6), 1635–1644.

Saxena, T., Karumbaiah, L., Gaupp, E. A., Patkar, R., Patil, K., Betancur, M., Stanley, G. B., & Bellamkonda, R. V. (2013). The impact of chronic blood-brain barrier breach on intracortical electrode function. *Biomaterials*, *34*(20), 4703–4713.

Sloots, J. J., Biessels, G. J., & Zwanenburg, J. J. M. (2020). Cardiac and respiration-induced brain deformations in humans quantified with high-field MRI. *NeuroImage*, *210*, 116581.

Steinmetz, N. A., Zatka-Haas, P., Carandini, M., & Harris, K. D. (2019). Distributed coding of choice, action and engagement across the mouse brain. *Nature*, *576*(7786), 266–273.

Tervo, D. G. R., Proskurin, M., Manakov, M., Kabra, M., Vollmer, A., Branson, K., & Karpova, A. Y. (2014). Behavioral variability through stochastic choice and its gating by anterior cingulate cortex. *Cell*, *159*(1),

21–32.

The International Brain Laboratory, Aguillon-Rodriguez, V., Angelaki, D. E., Bayer, H. M., Bonacchi, N., Carandini, M., Cazettes, F., Chapuis, G. A., Churchland, A. K., Dan, Y., Dewitt, E. E., Faulkner, M., Forrest, H., Haetzel, L. M., Hausser, M., Hofer, S. B., Hu, F., Khanal, A., Krasniak, C. S., … Zador, A. (2020). A standardized and reproducible method to measure decision-making in mice. In *bioRxiv* (p. 2020.01.17.909838). https://doi.org/10.1101/2020.01.17.909838

Wellman, S. M., & Kozai, T. D. Y. (2017). Understanding the inflammatory tissue reaction to brain implants to improve neurochemical sensing performance. *ACS Chemical Neuroscience*, *8*(12), 2578–2582.

Wood, F., Black, M. J., Vargas-Irwin, C., Fellows, M., & Donoghue, J. P. (2004). On the variability of manual spike sorting. *IEEE Transactions on Bio-Medical Engineering*, *51*(6), 912–918.

Zhou, R., Li, Y., Cavanaugh, J. M., & Zhang, L. (2020). Investigate the variations of the head and brain response in a rodent head impact acceleration model by finite element modeling. *Frontiers in Bioengineering and Biotechnology*, *8*, 172.